ADDIS ABABA UNIVERSITY

SCHOOL OF GRADUATE STUDIES

ADDIS ABABA INSTITUTE OF TECHNOLOGY

SCHOOL OF CHEMICAL AND BIO ENGINEERING

Removal Of Arsenic(III) from Aquoes Soloutions by Carboxy-Methyl Cellulose-Stabilized Nano Zero-Valent Iron

Nahom Kahsay

Advisor Dr. Eng. Hundessa Dessalegn

A thesis submitted to the School of Chemical and Bio Engineering

Presented in Fulfillment of the Requirements for the Degree of Master of Science (Process Engineering)

Addis Ababa

University

Addis Ababa,

Declaration

This is to certify that the thesis is prepared by Nahom Kahsay, entitled: **Removal Of Arsenic (III) from Aquoes Soloutions by Carboxy-Methyl Cellulose-Stabilized Nano Zero-Valent Iron** and submitted in partial fulfillment of the requirements for the Degree of Masters of Science in Process Engineering complies with the regulations of the University and meets the accepted standards with respect to originality and quality.

MSc Thesis

Approved by Board of Examiners

Dr. Eng. Hundessa Dessalegn

Advisor	Signature	Date
_____	_____	_____
Internal Examiner	Signature	Date
Dr Lemma Dendena	_____	_____
External Examiner	Signature	Date
Dr Ing Berhanu Assefa	_____	_____
Chair person, school graduate committee	Signature	Date
Dr Eng Abubeker Yimam	_____	_____

ABSTRACT

Arsenic is the most hazardous element in the chemical world and its presence in drinking water can cause disaster. Conventional method of preparation of nano zero valent iron using physical and chemical methods normally employ toxic chemicals as reducing agents, organic solvents, or non-biodegradable stabilizing agents, and are therefore potentially dangerous to the environment and biological systems. Experiments were conducted in a batch system and the effects of pH, contact time, and the initial concentrations of Arsenic (III) and nanoscale zero valent iron doses were investigated. The nature and morphology of synthesized adsorbent were characterized by X-ray diffraction and Fourier transform infrared spectroscopy. The experimental results revealed that the removal efficiency of Arsenic (III) was increased with decreasing pH of the solution but decreased with gradual increasing of initial concentration and dosage. The removal rate of Arsenic (III) was 97.4 % at a dosage of 1.0 g, pH 2 and with 15g/L initial As(III) concentration. The experimental data was found to be well described by Langmuir model. The maximum loading capacity as estimated by Langmuir model was 116.27 mg/g. Also, the adsorption trend followed the pseudo-second order kinetics model and equilibrium was achieved in two hours. Overall, the results obtained indicate that CMC-Stabilized nZVI could be effectively used for removal of Arsenic (III) from waste water.

Keywords: Arsenic; nano zero valent iron; Adsorption

Acknowledgements

Above all, praise to almighty God, lord of creations, and the most merciful and compassionate who blessed me with prospective ability to attain my task in this research work.

I would like to thank my advisor Dr.Eng. Hundessa Dessalegn for his indispensable, prompt help and invaluable effort in guiding and supervising during the course of this thesis. I treasure his advice which has contributed a great deal to the success of this work. Had it been not for his advice, the accomplishment of the thesis work would have been impossible.

I want to thank and express my heart felt gratitude to all technical staff members of Addis Ababa Institute of Technology, School of chemical and Bio Engineering.

My deepest gratitude also goes to Dr. yonas and Mr Debebe who kindly support in completing the lab work at College of Natural and Computational Science, Department of Chemistry.

Finally, I would like to extend my deepest sense of gratitude to my family and friends for their support and encouragement in successful completion of this thesis.

Table of Contents

List of Figures

List of Tables

List of Acronyms

As (VI)	Arsenate
As (III)	Arsenite
EPA	Environmental protection agency
FTIR	Fourier Transform Infrared Spectroscopy
nZVI	Nano Zero-Valent Iron
XRD	X-ray diffraction
WHO	World Health Organization
DI water	Distilled water
CMC	Carboxyl-methyl cellulose
SEM	Scanning Electron Microscope
DLVO	Derjaguin-Landau-Verwey-Overbeek theory
ORP	Oxidation-reduction potential
GAE	Gallic acid equivalents
GT-Fe NPs	Green tea iron nano particles

CHAPTER ONE

1. INTRODUCTION

1.1. Background of the Study

Heavy metals like arsenic, copper, cadmium, chromium, nickel, zinc, lead, and mercury are major pollutants of fresh water reservoirs because of their toxic, non-biodegradable, and persistent nature. The industrial growth is the major source of heavy metals introducing such pollutants into different segments of the environment including air, water, soil, and biosphere(Azimi.,2017)

Arsenic is the most pollutant element in the chemical world because of its high toxicity and carcinogenicity. Chronic exposure to arsenic may cause tumors in the liver, lung, kidney, bladder, skin, and various human tissues, lead to cardio vascular system problems and impede the mental development of children. The World Health Organization has lowered the limit of arsenic concentration in drinking water from 50 to 10 mg /L(Gautam and Gupta 2009).

Toxicity, mobility, and bioavailability of arsenic is related to its chemical speciation, oxidation state, and solution pH. In natural water, arsenic exists mainly as the inorganic arsenate As(V) and arsenite As (III). As(V) predominates in oxidizing conditions and is present mainly as H_3AsO_4 (pH <2.2), $H_2AsO_4^{-1}$ (2.2 < pH < 7), $HAsO_4^{2-}$ (7 < pH < 11.5), and AsO_4^{3-} (pH > 11.5). As(III) is the major arsenic species under reducing conditions and is present mainly as neutral H_3AsO_3 ,(pH < 9.2), $H_2AsO_3^{-}$ (9.2 < pH < 12), and H_2AsO3^{2-} (pH > 12)(Cheng , 2016).

Adsorption is one of the most promising techniques for arsenic removal from water, and iron oxide is used extensively as an adsorbent because of its high affinity toward arsenic and low cost. Recently, nanomaterials have been suggested as efficient, cost-effective and environmental friendly in the removal of As ion from aqueous solution (Bezza and Chirwa , 2018).

Nano zero Valent Iron has recently become the most common metallic reducing agent (reductant) for environmental applications due to its abundance, low toxicity, low cost and effectiveness(Nayana and Pushpa , 2016). nZVI is a kind of reactive transition metal with reductive property (standard redox potential, E0h = −0.44 V). It can directly transfer electrons to the contaminants and transform contaminants into non-toxic or less toxic species during

the remediation processes. Many studies have reported that nano zero valent iron (nZVI) with a higher adsorption capacity is effectively used at low concentrations to remove chrome and arsenic as heavy metals (Ulucan-Altuntas, Debik and Gungor , 2018).

Orange peels contains high concentration of polyphenols which makes orange as high antioxidant source, it can be used as a reducing agent during the synthesis of Nano Zero Valent Iron. Orange peel is about half of the total fruit weight and is very rich in pigments. The color of the orange peel generally comes from phenolic compounds and carotenoids. As the phenolic compounds in the peel increase, redness in the peel decreases and jaundice increases(P, Kodal S,2017).

1.2. Statement of the Problem

Conventional method of preparation of Nano zero valent iron using sodium borohydride reduction method has lot of limitations. Firstly, the cost of nanoscale ZVI is relatively high due to price of sodium borohydride. Secondly, it releases toxic substances to the environment, Moreover, its relatively unstable which means production, transport and usage require careful control. Furthermore, it produces large quantities of explosive hydrogen gas as a result of additional safety protocols required for dealing with the gas on a large scale to produce(Kozma, Gábor, Andrea Rónavári, Zoltán Kónya, and Ákos Kukovecz,2016).

New approaches are continuously being developed as a means replacing of this traditional method (sodium borohydride reduction method) by natural reducing agent like polyphenol. Production of nanoparticles from the extracts of orange peel which is rich in polyphenol, is very simple to synthesis, cost-effective and no hazardous effects on the environment.

In this study, the effects of pH values, Initial As (III) concentrations and dosage were examined to investigate the removal efficiency of carboxy-methyl cellulose-stabilized nano zero-valent Iron particles

1.3. Objectives

1.3.1. General objective

The General objective of this study is synthesizing carboxy-methyl cellulose-stabilized nano zero-valent Iron particles using polyphenol extract from orange peel for the removal of Arsenic (III) from aqueous solution.

1.3.2. Specific Objectives

1. To extract and characterize the orange peel extract

2. To synthesize CMC –Stabilized nZVI using orange peels extract as reducing agent.

3. To characterize the CMC- Stabilized nZVI particles using X-Ray Diffraction (XRD), Fourier Transform Infrared Spectroscopy (FTIR) and Scanning Electron Microscope to determine crystalinity, functional groups and morphology of CMC-Stabilized Nano Zero Valent Iron respectively.

4. To determine the impact of adsorption kinetics and Adsorption Isotherm during removal process.

5. To investigate the effect of various parameter such as pH, dosage and initial Concentration on the removal efficiency and also to find the optimum condition.

1.4. Significance of the study

- Results from this study can be used to assess the utility of the green synthesis of nZVI .
- These nZVI could be utilized for the heavy metal removal, in particular for Arsenic
- This study will enhance the economic value of the orange peels, during the extraction of Polyphenols.
- Replacing the conventional reducing agent with Polyphenol adds to the advantage.
- Utilization of orange peels as source antioxidants will reduce the ecological burden of society (pollution) and have considerable economic benefit to food process.

CHAPTER TWO

2. LITERATURE REVIEW

2.1. Nano Zero Valent Iron

For decades, zero-valent iron technology has been extensively developed for environmental contaminant remediation because iron is abundant, cost-effective, and environment friendly and the remediation process is easily manipulated. nanoscale zero valent iron (nZVI) is a composite consisting of Fe (0) and ferric oxide coating. nZVI nanoparticles were found to possess a core–shell structure composed of a metal iron core encapsulated by an iron (oxyhydr)oxide shell. The metallic iron as electron donor offers a reductive character, while the oxide shell permits solute adsorption via electrostatic interactions and/or surface complexations, facilitating or inhibiting electron transfer from the metal core to the outside shell (Suponik, Lemanowicz and Wrona , 2016).

Besides, the particle size of nZVI is controllable and there are abundant reactive sites on the surface. The high reducing capacity and large specific surface area contribute to the superior performance of nZVI in removing heavy metals from wastewater. It has received increased attention as a novel adsorbent to treat various kinds of heavy metals, such as Hg (II), Cr (VI), Cu (II), Ni (II), Cd (II), etc. since it came out(Yang , 2019).

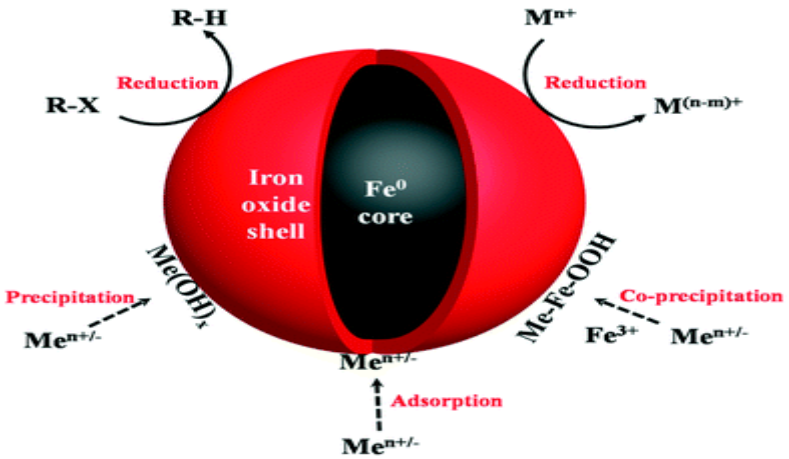

Figure 1: Illustration of oxide shell mediated contaminant removal by nZVI (Mu, Yi, Falong Jia, Zhihui Ai, and Lizhi Zhang ,2017)

2.2. Oxide Shell Formation Mechanism of nZVI

The amorphous shell was mainly composed of iron oxides, which were formed *via* corrosion of the iron core by water, oxygen, and substrates during the nZVI synthesis process when synthesized under solvent-free conditions, a "bare" nZVI exposed to air is prone to be oxidized. Fe^{2+} is a primary product and then can undergo further oxidative transformation to generate Fe^{3+}. Fe^{3+} could react with OH^- to yield $Fe(OH)_3$, which may further dehydrate to form oxyhydroxide (FeOOH) . These two ferric products ($Fe(OH)_3$ and FeOOH) prefer to precipitate on the surface of nZVI(Chandra and Khan , 2017).

When synthesized under solvent-free conditions, a "bare" nZVI exposed to air is prone to be oxidized. The oxidation process is very rapid and takes about 0.2 fs to form an initial 1 nm thickness of oxide layer on a freshly exposed iron surface at room temperature according to the Cabrera–Mott model, It should be noted that only particles larger than 8 nm possess a core–shell structure with the surface oxide layer of a typical thickness of ∼3 nm. If the particle sizes are smaller than 8 nm, the overall particles would be fully oxidized(Vijayakumar, Tamilarasan, and Dharmendirakumar 2012).

$$2Fe^0(s) + 2H_2O(L) \longrightarrow 2Fe^{2+} + H_2(g) + 2OH(aq) \quad (2.1)$$

$$2Fe^0(s) + 2H_2O(L) \longrightarrow 2Fe^{3+} + H_2(g) + 2OH(aq) \quad (2.2)$$

$$2Fe^{3+} + 3OH^- \longrightarrow Fe(OH)_3 \quad (2.3)$$

$$Fe(OH)_3 \longrightarrow FeOOH + H_2O \quad (2.4)$$

$$FeOOH \longrightarrow Fe_2O_3 + H_2O \quad (2.5)$$

The oxide shell's porosity can affect the contaminant transfer to the Fe^0 core surface. Generally, organic contaminants could co-precipitate with iron corrosion products (oxides/hydroxides) and absorb onto the surface of the oxide shell during the nZVI based pollutant removal process. Once absorbed on the surface of the oxide shell, the contaminants could transfer across the oxide shell and migrate to the nZVI iron core with a lower valence state of iron. The contaminants' transfer across the oxide shell depended on the concentration gradients of contaminants, and the porous structures of the oxide shell could facilitate the contaminants' transfer across the oxide shell. Ideally, contaminants transferred across the porous oxide shell to the iron core surface, where they were reduced by Fe^0 directly (Mu, Yi, Falong Jia, Zhihui Ai, and Lizhi Zhang ,2017).

However, nZVI is highly susceptible to corrosion in aqueous solution, followed by the generation of Fe (II) from the core iron corrosion. The newly formed Fe (II) would transfer across the oxide shell in the opposite direction to contaminant transfer, and the contaminant reduction could occur at the meeting point within the oxide shell. Goldberg's research results suggested that the contaminant reduction within the oxide shell was thermodynamically more favorable than at the iron core surface. Therefore, the contaminant reduction preferred to occur within the oxide shell rather than at the Fe^0 core surface. Reductive degradation of organic contaminants also depended on the indirect electron transfer from the iron core to the adsorbed contaminants through the oxide shell (Yang , 2019).

Generally, iron oxides are considered as an n-type semiconductor; electro migration in the iron oxides is correlated with the energy required to excite an electron from the valence band to the conduction band (i.e. E_g). nZVI is able to effectively remove various heavy metal ions, including Cr^{6+}, Ni^{2+}, Hg^{2+}, Pb^{2+}, Cu^{2+}, Zn^{2+}, Ba^{2+}, Cd^{2+}, UO_2^{2+}, and Se^{6+}, and inorganic ions, As(V)/As(III). The removal mechanisms of heavy ions with nZVI are mainly related to the standard redox potential (E^0_h) of the metal ion shell.(Mu, Yi, Falong Jia, Zhihui Ai, and Lizhi Zhang ,2017)

Metals with E^0_h more positive than that of Fe^0 (e.g., Cr^{6+}, Cu^{2+}, UO_2^{2+}, and Se^{6+}) are preferentially reduced into lower valence states when they are absorbed on the oxide shell and then co precipitate with iron oxides/hydroxides, and these metal ions could also be removed *via* sorption/surface complex formation with iron corrosion products. For the metals (e.g., Zn^{2+}, Ba^{2+}, Cd^{2+}) with E^0_h more negative than that of Fe^0, they are removed by the adsorption to the iron oxide shell. It should be noted that the adsorption, the redox reaction, and the co-precipitation mainly occurred on the nZVI surface (Mu, Yi, Falong Jia, Zhihui Ai, and Lizhi Zhang ,2017).

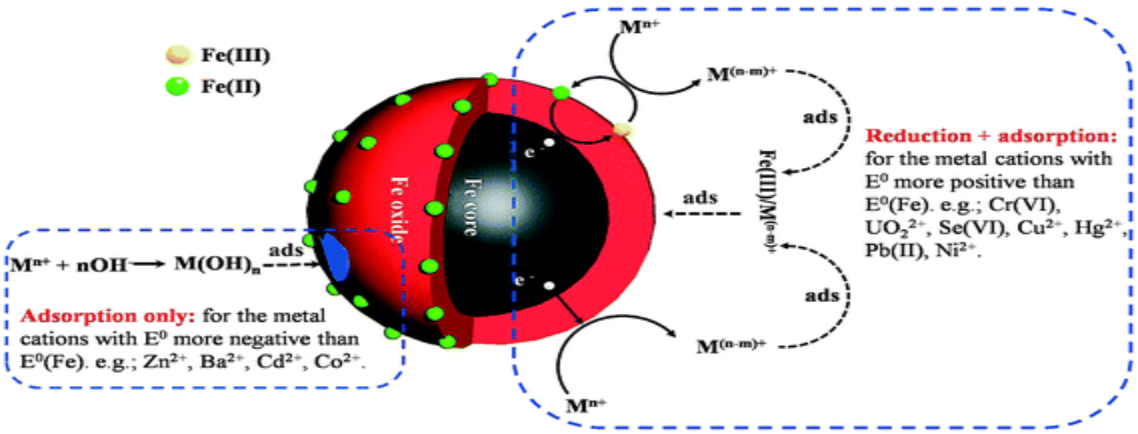

Figure 2: Illustration of heavy metal removal by nZVI (Mu, Yi, Falong Jia, Zhihui Ai, and Lizhi Zhang ,2017)

2.3. Aging

The oxide film growth was usually accompanied by oxyhydroxide aging, resulting in the increase in oxide shell density and the decrease in oxide shell porosity, significantly limiting the contaminant transfer and thus inhibiting reductant and contaminant interactions due to exposer to the atmosphere. The reactivity loss of aged nZVI was attributed to the recovery (a process by which deformed grains can reduce their stored energy through the removal or rearrangement of defects in their crystal structure) and recrystallization of the oxide shell. Aging in the atmosphere was considere as a limiting factor in the use of nZVI to reduce groundwater contaminants**.** However, vacuum drying without aging in the atmosphere can maintain the amorphous structure of the oxide shell, allowing nZVI to be rapidly oxidized along with a significant decrease in reactivity(Yang , 2019).

2.4. Stability Issues

Nanoparticles have been proven to be effective in the adsorption of heavy metals. However, since they are usually present as fine or ultrafine particles, nanoparticles have low energy barriers, causing them to aggregate and achieve a stabilized state. Aggregation decreases the free surface area of the nanoparticles, thereby reducing their adsorption capacity and reactivity. Moreover, the mobility of the particles decreases, which further contributes to reducing their effectiveness. To overcome the problems associated with aggregation, two solutions were reported in literature. A first solution is the impregnation of nanoparticles into porous materials or surface coatings. Some of the widely used host substrates are activated carbon, bentonite, sand, alumina membranes, and ion-exchange resins. As for surface coating, there have been reports mentioning that a thick layer of surface modifiers may reduce the reaction rate, although removal capacity was enhanced due to an increased number of active sites. Thus, tradeoff between stability and reactivity must be studied well(Nicomel , 2015).

2.5. Regeneration and Reuse

In cases where process economy dictates that immediate disposal is not cost-effective, regeneration of the adsorbent seems to be the preferred option. Several studies suggest that the maximum adsorption capacity of metal-based nanoparticle adsorbents remains almost constant after several cycles of regeneration and reuse. Moreover, pH is considered as an important factor in the desorption of metals from the adsorbents. Concerning the desorption

characteristics of arsenate and the recovery of the adsorbent maghemite (γ-Fe_2O_3) nanoparticles. Among the five alkaline solutions studied (i.e., NaOH, Na_2CO_3, Na_2HPO_4, $NaHCO_3$, and NaOAc), 0.1 M NaOH showed the highest desorption efficiency of 90%. Moreover, desorption was proven to be affected by pH and the concentration of the alkaline solution. By increasing the concentration of NaOH to 1 M, full desorption of arsenate was achieved. Although using nZVI to remove heavy metal has many advantages, its shortcomings cannot be neglected. NZVI was reported to be oxidized with oxygen and water in an aqueous solution, slowing down or hindering the reduction process of the heavy metals. nZVI was also reported to aggregate easily, resulting in the decrease of the reaction surface area and mobility. Besides, the separation of nZVI from wastewater is difficult. In order to improve the performances of the nZVI, various kinds of modification strategies have been developed, such as surface chemical modification or doping nZVI with other metals (Pd, Cu, Ni, Pt etc.). For example, Huang et al. synthesized a novel nZVI-modified material by combing nZVI with sodium dodecyl sulfate (SDS) which is one kind of anionic surfactant and possesses excellent abilities of migration and dispersion(Nicomel , 2015) .

2.6. Disposal of Arsenic (III) Contaminated Nanoparticles

The nanoparticles may need to be disposed when their saturation capacity is reached. For other metals and organics, nanoparticles may be recovered through combustion. However, in the case of arsenic-loaded materials, combustion may not be ideal as arsenic oxides are volatile and are easily released to the atmosphere during the combustion process, which creates a new environmental hazard. Therefore, the most attractive option to handle arsenic-loaded nanoparticles currently seems to be encapsulation through stabilization-solidification, followed by secure landfill disposal. The first step, stabilization-solidification, is a popular technique used to convert a potentially hazardous liquid or solid waste into a less or non-hazardous waste before it is disposed in secure landfills (Nicomel, 2015).

2.7. Synthesis of Nano Zero Valent Iron using Sodium brohydroxide

The preparation of Nano-Zero Valent Iron is normally conducted in two ways; by heating process using a mixture of iron oxide and carbon and lime powder or by reduction of dissolved iron using a reducer to transform the dissolved metal into zero-valent iron .Production of ZVI involved a reduction method using two main chemicals which were $FeCl_2.4H_2O$ and $NaBH_4$ .The NaBH4 functions as a reducing agent in order to reduce the iron

chloride (FeCl2.4H2O) in form of solution to produce zero valent iron. The method comprised of four stages which were mixing, separating, washing and drying(Yaacob, Kamaruzaman, and Samsudin 2012).

2.8. Recent Research Development on Green synthesis of Nano Zero Valent Iron

Chemical synthesis methods (e.g., chemical reduction, sol gel technique, etc.) involve the usage of toxic chemicals, formation of hazardous byproducts, and contamination from precursor chemicals. Hence, there is a growing need to develop clean, nontoxic, and environment-friendly procedures for nanoparticle synthesis. Some of the distinct advantages that biological synthesis protocols have over the conventionally used physical and chemical methods are(a)clean and eco-friendly method, as toxic chemicals are not used ;(b)the active biological component like enzyme itself acts as a reducing and capping agent, thereby reducing the overall cost of the synthesis process;(c)small nanoparticles can be produced even during large-scale production;(d)external experimental conditions like high energy and high pressure are not required, causing significant energy saving. , plant-mediated biological synthesis of nanoparticles has gained importance only in the recent years(Kozma, Gábor, Andrea Rónavári, Zoltán Kónya, and Ákos Kukovecz,2016).

Synthesized iron nanoparticles, GT-Fe NPs (consisting mainly of iron oxide/oxohydroxide), using green tea extract. These nanoparticles served as Fenton-like catalyst for the degradation of cationic dyes such as methylene blue (MB) and anionic dyes like methyl orange (MO). Almost complete removal of both dyes was achieved in 200 and 350 minutes for MB and MO, respectively. In the case of GT-Fe NPs, almost 100% removal of MB and MO was observed at an initial dye concentration of 10 mg/L and 100 mg/L (Shahwan, 2011).

Used aqueous Sorghum sp. (hybrid sorghum) bran extract for nZVI synthesis. The extract was prepared by obtaining sorghum bran powder in double-distilled water at different temperatures for half an hour. UV-visible spectra for these nanoparticles were similar to those for nZVI synthesized by tea polyphenols. Based on the XRD pattern, the nanoparticles were found to be amorphous in nature. The catalytic activity for the degradation of bromothymol blue was found to be higher for higher concentration of nanoparticles (Njagi, 2011).

Iron nanoparticles using eucalyptus leaf extract by adding 0.1 M $FeCl_3$ solution in a ratio of 1: 2. The lack of any distinct diffraction peak indicated that the as-synthesized nanoparticles

were amorphous in nature. An azo dye, acid black 194, was used to test the adsorption-flocculation capacity of nanoparticles. As-synthesized nanoparticles exhibited very high adsorption-flocculation capacity and, at 25°C, 1 gm of nanoparticle removed 1.6 gm of the organic dye acid black 194 (Wang, 2009).

nZVI using grape marc, black tea, and vine leaf extract. The degradation efficiency of the synthesized nanoparticles tested against the commonly used anti-inflammatory drug ibuprofen. In aqueous solution, at initial concentration of 10 mg/L and pH at 7 iron nanoparticles synthesized using black tea showed degradation efficiency of 51 to 66%. At pH 3, efficiency of nZVI synthesized using black tea extract decreased by 30%. The efficiency was 32% and 42% for grape marc and vine of the leaf extract nZVI, respectively (Machado, 2013).

Peel extract as a low-cost bio- reducing agent for synthesizing magnetite nanoparticles. Iron salt solution was hydrolyzed, resulting in the formation of ferric hydroxide, which was subsequently reduced by various biomolecules to form Fe_3O_4 nanoparticles (Venkateswarlu, 2012). Utilization of ultrasound technique to decompose volatile precursors in solvent with low vapour pressure has a lot advantages. This method of sensitizing nZVI can be easily operated at room temperate and very cost effective. However, it has significant limitation in productivity and agglomeration (Suponik, Lemanowicz, and Wrona 2016).

Nanoparticles have the tendency to aggregate which can reduce the effectiveness of nano particles. The ability of nanoparticles to serve as a versatile application tool could be attributed to their unique physicochemical characteristics that significantly differ from their bulk counterparts. Nevertheless, their tendency toward aggregation results in reduced reactivity and longevity, which in turn exerts negative impact on their application potential. To overcome this constraint, several surface modifications and particle stabilization methods have been developed using various kind additives such as surfactants, polymers, water-soluble starch, carboxymethyl cellulose, cellulose acetate, polyacrylic acid, etc(Yaacob, Kamaruzaman, and Samsudin 2012).

The primary aims of this research were to sensitize nZVI by reduction of iron chloride using polyphenol from orange peel extract with excellent efficiency. This method has many advantages, which operated at ambient conditions; low agglomeration and environmentally friendly. Moreover, to prepare a CMC-stabilized nZVI suspension through a chemical reduction method for removal of As (III) in an aqueous solution, considering the physical

stability and chemical reactivity of the suspension in the nZVI. The CMC compounds can enhance particle stability because of the presence of carboxyl functional and hydroxyl groups in cellulose networks. The phenomenon also requires the stabilization of the nZVI surface during synthesis. The stabilization technique involving the use of polar anchoring groups (e.g., –COOH, –OH, and –CO) and stabilizing hydrocarbon chains potentially inhibits the aggregation of nZVI particles through long-range steric forces and electrostatic stabilization which suppress particle agglomeration.

CHAPTER THREE

3. MATERIALS AND METHODS

3.1. Materials

3.1.1. Raw material

Fresh orange collected from Upper Awash Fruit and Vegetable Industry Enterprise. It was from Citrus Sinesis var. Valencia.species.

3.1.2. Chemicals

Chemicals like hydrochloric acide, methanol, Folin Ciocalteu Reagent, Gallic acid, Iron chloride ($FeCl_3$), Hydrochloric acid (HCl). Sodium Arsenite were used during the investigation of the laboratory works. Sodium Arsenite and methanol were bought from Charkos Market Center, but all other listed chemicals were available in School of Chemical and Bio Engineering, Addis Ababa Institute of Technology, Addis Ababa University.

3.1.3. Apparatus

Apparatus like Knife Cutter, Oven dryer, Electrical grinder, burette, Triple neck round bottom flask, conical flask, centrifuge, overhead stirrer, Whatman filter paper, Rotary vacuum evaporator, FTIR (Perkin Elmer, Spectrum 65FT-IR spectrophotometer) and 725nm using a UV-Visible Spectrophotometer (UV-7804C) were used during laboratory work. Knife cutter and Whatman filter paper were bought from the Market, oven dryer, conical flask, rotary vacuum evaporator was used in the School of Chemical and Bio Engineering, Addis Ababa Institute of Technology, Addis Ababa University and UV-Spectrophotometer were used in the Center of Food and Nutrition, College of Natural Science, Addis Ababa University.

Table 1 . Chemicals and their Function

Chemicals	Function
Metanol	As extraction solvent
Folin- Ciocalteu reagent	Reagent used for determination of polyphenol
Gallic acid	Positive control or standard for phenol determination
Sodium Arsenite	Source for heavy metal As(III) ion
Sodium carbonate	For prevention of precipitation and turbidity of reagent during polyphenol determination
Iron Chloride	Standard for radical scavenging activity
Carboxyl-methyl cellulose	Stabilizer agent

Table 2. Apparatus and their function

Apparatus	Function
Triple necked round bottom flask	To sensitize Zero valent Iron
Oven dryer	To dry wet peels
Knife	To reduce the size of peels in to pieces
Electric grinder	To obtain powder
Centrifuge	To concentrate the nZVI adsorbent produced
Filter paper	To isolate the supernatant from residue
Rotary evaporator	To remove solvent from extract
Spectrophotometer (UV)	To determine absorbance of solution

3.2. Extraction of polyphenol from Orange Peels

3.2.1. Preparation of Orange Peels

Orange fruits were washed, hand peeled, the peels were cut into small slices, then dried in solar energy and grounded into fine powder with a mortar and pestle.

3.2.2. Polyphenol Extraction

Extraction was carried out by maceration method by using 10 g of the dried powder was soaked in 400 ml of methanol-water binary mixture solvent in conical flask, plugged with cotton wool and then kept in shaker at 120 rpm for given time, at given temperature. After

extraction time was completed, the extract was filtered through Whatman filter paper No.41 for removal of peel particles and concentrated under rotary vacuum evaporator at 40 ºC. The dry extract was stored at 4 ºC (Singh, 2014).

3.2.3. Preparation of Nano Zero valent Iron

A 0.1 M solution of ferric chloride was prepared by dissolving a fixed amount (2.703 g) of ferric chloride ($FeCl_3 \cdot 6H_2O$) in 100 mL of distilled water. The water used was pre-cooled to a temperature of 2-5 ºC for 30 minutes to decrease the amount of dissolved Oxygen which might consume the reducing agent. The synthesis process of green ZVI was based on the method (Njagi, 2011).

The ferric chloride solution was stirred for five minutes and then placed in a triple-neck flask. Varying amounts of orange peel extract was placed in a burette which was added to the ferric chloride solution by drop-wise addition to control the flow rate of the reducing agent. During the addition of the extract, the mixture was reached at 40ºCin the presence of vigorous magnetic stirring which stayed for 15 minutes which results rapid formation of fine black precipitates. The CMC-stabilized nZVI particles were synthesized through the chemical reduction method as reported by He and Zhao (F. He, D. Zhao,2007). The 1.0 L CMC stock solution at a concentration of 1.2% (w/w) was prepared by dissolving the CMC powder in Deionized water (DI) water. Probe-ultrasonication was conducted to the CMC-stabilized nZVI suspension for around 15 min by using a probe horn sonicator at 50% amplitude power. The suspension was then immediately used for the characterizations. The formation of colloids nZVI investigated with observation of the color change of the solution. The emergence of black color in the reaction showed the formation of nZVI. The resulting solution was then filtered by vacuum filtration for 30 min. Then after the generated precipitate was dried in an oven at 50°C for 24 hours. The particles were washed 3 to 4 times with a 4-10 M HCl (pH 4) solution and kept in a refrigerator at <4◦C.

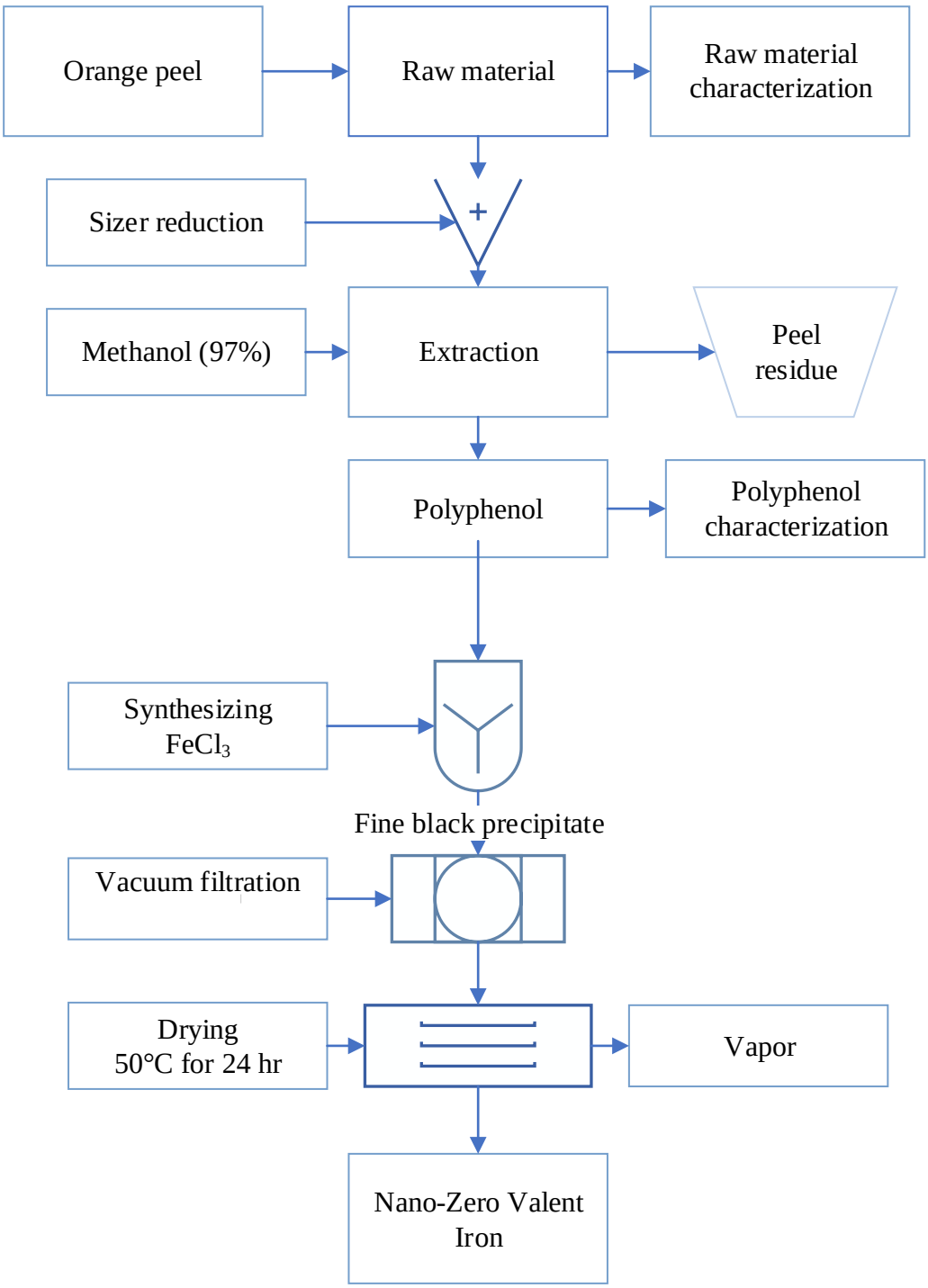

Figure 3: experimental procedure for Synitisise of Carboxyl-methyl Cellulose-Stabilized nZVI

3.3. Moisture Determination of orange peel

To determine the % moisture contents of the orange peel sample, 30 g sample was taken in a clean and dry crucible (W1) and kept in an oven at 50ºC for 24 hrs. The sample was then transferred desiccators to cool and weight, again it was transferred in to an oven until

constant weight after drying was obtained (W2) and % moisture was determined by following the formula:

$$\text{Moisture content (\%)} = \frac{W1-W2}{W1} * 100 \quad (2.6)$$

3.4. Ash content of orange peel

20g of dry orange peel was measured and placed into the muffle furnace and burnt for 4 hours at a temperature of 550 ºC and ignited until light gray ash was obtained (or to constant weight). Then after the sample was then cooled in a desiccator and weighed. Ash is the inorganic residue remaining after the water and organic matter have been removed by ignition or complete oxidation of organic matter in the presence of oxidizing agents, which provides a measure of the total amount of minerals within orange peels.

The ash content was expressed as:

$$A = 100 * (\frac{WA}{WB}) \quad (2.7)$$

Where A= ash content, WA=Mass of Residual, WB= Mass of the sample

3.5. Determination of total phenol content

The total phenol content was determined by an appropriate dilution of the extracts were oxidized by 2.5 mL Folin-Ciocalteau's with 10 mL distilled water and neutralized by 7.5% (V/V) sodium carbonate. The reaction mixture was incubated for 40 min at 45 °C and the absorbance was measured at 765 nm using a UV-Visible Spectrophotometer (UV-7804C).). The total phenol content was subsequently calculated as gallic acid equivalent. Hence, the more rapidly the absorbance increases, the more potent the antioxidant activity of the extract. Gallic acid was used as a positive control. A total phenol value was expressed in terms of Gallic acid equivalent (mg of Gallic acid/g of extracted compound) (Singh, 2014).

The total phenol content was calculated using the following relationship

$$T=\frac{C*V}{W} \quad (2.8)$$

Where C= Gallic acid equivalent concentration obtained from the calibration curve (mg/ml) V= volume of stock solution of extract (ml), W = dry weight of extract found in the stock solution (g) T = total phenol content (mg of GAE/g dry extract)

3.5.1. Reagent preparation

$NaCO_3$ reagent solution was prepared by weighing 7.5g of NaCO3& dissolving in 100ml distilled water using incubate at room temperature for 24 hours. Folin-Ciocalteu‟s reagent solution was prepared by taking 1ml of Folin-Ciocalteu‟s into 10ml of distil water.

3.5.2. Preparation of standard solution

Gallic acid was used as a standard for determination of total phenolic content of the extract and the total polyphenols were expressed as mg/g gallic acid equivalents (GAE) from the calibration curve. A stock solution (0.0125mg/ml) of Gallic acid was prepared by weighing 2.5g of Gallic acid and dissolving by 50ml of methanol in volumetric Measuring flask. A standard Gallic acid were withdrawn from the stock solution such as 20, 40, 60, 80, 100 and 120µL and mixed with 980, 960, 940, 920 ,900 µLand 880µL of methanol solvent to get Gallic acid concentrations of 1.0, 2.0, 3.0, 4.0 and 5.0 mg/mL respectively in separate test tubes.

3.5.3. Preparation of Standard Solution

50µL sample of orange peel extract, 50 µL of methanol and 1 mL of Folin-Ciocalteu‟s reagent was added, mixed well and incubated at 4^oC for 30 min. After 3 min, 1ml of saturated Na_2CO_3 solution was added and adjusted the solution to 7ml distilled water mixed well and incubated in the dark for 40 min at room temperature. After 40 min incubation, the absorbance was measured against at 725nm using a UV-Visible Spectrophotometer (UV-7804C). The experiment was carried out in triplicate. The total phenol content was calculated and expressed as milligrams of Gallic acid equivalents (mg of GAL/g dry extract) using the Gallic acid calibration curve and the curve used to determine the corresponding Gallic acid concentration of the samples.

3.6. Characterization of Nano Zero Valent Iron

3.6.1. Fourier Transform Infrared Spectroscopy (FTIR) analysis of nZVI

FTIR analysis was performed to identify the existence of surface functional groups in the Nano Zero valent iron. The functional groups of the Adsorbent before and after sorption were determined using Spectrum 65 FT-IR (PerkinElmer) in the wave range 4000 - 400 cm-1 using KBr pellets.

3.6.2. X-Ray Diffraction (XRD) analysis of nZVI

XRD is a simple, versatile, non-destructive and comparatively inexpensive technique for identifying the phases of crystalline materials. These techniques are based on observing the scattered intensity of an X-ray beam hitting a sample as a function of incident and scattered angle, polarization, and wavelength or energy.The Analytical instrument uses Cu Kα radiation and graphite monochromator to give X-rays with wavelength of 0.154060nm .

3.6.3. Scanning electron microscopy (SEM)

Scanning Electron Microscope used to qualitatively determine the morphology, size and composition of the samples. SEM analysis was performed for the non-and CMC-stabilized nZVI particles. Images of the nZVI surface were taken at different magnifications.

3.7. Determination of the amount of As(III) adsorbed from aqueous solution

The adsorption of Arsenic (III) by nZVI was conducted in batch mode. For each experiment, 250 mL of the As (III) solution of desired concentration was added into Erlenmeyer flasks. The desired pH for each experiment was adjusted using 0.1 M HCl and NaOH. Then, the predetermined dose of nZVI was added into the Erlenmeyer flask and the mixture was agitated at 150 rad/min speed by a shaker. After the 2hr contact time, the samples were filtered through vacuum filter and then dried in oven and the concentration was analyzed by analytical equipment's. The amount of adsorbed (mg/g) As(III) was calculated using the formulae reported by Vanderborght and Van Griekenm (Vanderborght, 1977).

$$Q = \frac{V\,(Ci - Cf)}{W} \qquad (2.9)$$

Where Q = the amount of solute adsorbed from the aqueous solution, V = Volume of the adsorbate, Ci = the concentration before adsorption, Cf = the concentration after adsorption and W = the weight in gram of the adsorbent. The removal efficiency was determined by computing the percentage sorption using the formulae

$$\% \text{ Sorption} = \frac{Ci - Cf}{Ci} \qquad (3.0)$$

The main process parameters studied were solution pH range (3, 6, 9), initial As (III) concentrations (10, 15, 20mg/L), adsorbent doses (0.5,1.0,1.5 g).All the experiments were conducted at room temperature in duplicated to ensure the reproducibility.

3.8. Effect of pH

The pH is one of the most critical parameters in the As (III) removal using nanoparticle zero-valent iron. In this experiment, the adsorption behavior of As (III) was studied at different pH (2,6,9), using 1g of nZVI particles with a fixed concentration of As (III) (15 mg/L)**.** pH influences the surface charge of the adsorbent, the degree of ionization and the species of adsorbate. So, the pH of the aqueous solution is an important controlling parameter in the heavy metal adsorption process.

3.9. Effect of Dosage

The effect of adsorbent dosage was studied at varying nZVI solid concentrations (0.5, 1, 1.5 g/L), maintaining initial Arsenic concentration 15g/L with at a pH of 6.

3.10. Effect of Initial As (III) Concentration

Studies on the effect of initial Arsenic concentration was performed at 10, 15, 20 mg/L, using 1 g nZVI and at a constant pH 6. The arsenic removal efficiency as a function of initial As (III) concentration with nZVI.

3.11. Sorption Isotherm

The performance of an adsorbent can be studied by adsorption isotherm data, which can be obtained by a series of experimental tests in labs. Modeling the adsorption isotherm data is an essential way for predicting and comparing the adsorption performance, which is critical for optimization of the adsorption mechanism pathways, expression of the adsorbents capacities, and effective design of the adsorption systems (Chen, 2015). Two-parameter isotherm models are commonly used in modeling the adsorption data, such as Langmuir and Freundlich (Bezza and Chirwa 2018). For adsorption Isotherm studies, 1g of the adsorbent was contacted with randomly selected initial As (III) concentrations of 7mg/L,33mg/L,130mg/L,150mg/L and 155mg/L and at pH of 3 with a contact time of 2hrs.

3.12.1. Langmuir Adsorption Isotherm

The Langmuir isotherm model is based on the assumption that there is a finite number of active sites which are homogeneously distributed over the surface of the adsorbent. These active sites have the same affinity for adsorption and there is no interaction between adsorbed molecules. The Langmuir isotherm is valid for monolayer adsorption onto a surface

containing a finite number of identical sites. The model assumes uniform energies of adsorption onto the surface and no transmigration of adsorbate in the plane of the surface. Based upon these assumptions,

Langmuir represented the following equation:

$$Q_e = \frac{Q_o K_L C_e}{1 + K_L C_e} \quad (3.1)$$

$$\frac{1}{Q_e} = \frac{1}{Q_o} + \frac{1}{C_e Q_o K_L} \quad (3.2)$$

$$\frac{C_e}{Q_e} = \frac{C_e}{Q_o} + \frac{1}{Q_o K_L} \quad (3.3)$$

Where:

Q_o = maximum monolayer coverage capacity (mg/g)

K_L = Langmuir isotherm constant (L/mg).

C_e = the equilibrium concentration of adsorbate (mg/L^{-1})

Q_e = the amount of metal adsorbed per gram of the adsorbent at equilibrium (mg/g).

The value Q_O and K_L were computed from the slope and intercept of the Langumer plot of

Ce/Qe versus Ce the essential features of the Langmuir isotherm may be expressed in terms of equilibrium parameter R_L Which is a dimensionless constant referred to as separation factor or equilibrium parameter

$$R_L = \frac{1}{1 + C_0 KL} \quad (3.4)$$

Where:

C_0 = Initial Concentration

R_L = Shape factor for adsorption Isotherm

R_L value indicates the adsorption nature to be either unfavorable if $R_L>1$), linear if R_L =1, favorable if $0< R_L<1$ and irreversible if $R_L=0$

3.12.2. Freundlich Adsorption Isotherm

The Freundlich isotherm model applies to adsorption on heterogeneous surfaces with interaction between the adsorbed molecules, and is not restricted to the formation of a

monolayer. This model assumes that as the adsorbate concentration increases, the concentration of adsorbate on the adsorbent surface also increases and, correspondingly, the sorption energy exponentially decreases on completion of the sorption centers of the adsorbent.

$$Qe = K_f Ce^{1/n} \quad (3.5)$$

Where K_f = Freundlich isotherm constant (mg/g)

n= adsorption intensity;

C_e = the equilibrium concentration of adsorbate (mg/L)

Q_e = the amount of metal adsorbed per gram of the adsorbent at equilibrium (mg/g).

Linearizing the above equation, we can have:

$$\text{Log } Q_e = \text{Log } K_f + \frac{1}{n} \text{Log } C_e \quad (3.6)$$

The constant K_f is an approximate indicator of adsorption capacity, while 1/n is a function of the strength of adsorption in the adsorption process.

3.13. Adsorption Kinetics Model

The kinetic parameters, which are helpful for the prediction of adsorption rate, give important information for designing and modeling the adsorption processes. It is necessary to study the kinetics of the process to investigate the factor influencing the reaction rate. Adsorption kinetics provide better understanding about the adsorption of arsenic (III) on the nZVI and producing a predictive model to estimate a number of ions absorbed during adsorption. In all kinetic experiments, the pH of the solution and dosage was kept at optimum 2 and 15 respectively, and the sample was taken at every 20 minutes.

3.13.1. Pseudo-First-Order Kinetic Model

The pseudo-first-order kinetic model can be shown as follows:

$$\frac{dQt}{dt} = (Q_e - Q_t) \quad (3.7)$$

Which can be rearranged to obtain a linear form:

$$\text{Log } (Q_e - Q_t) = \text{Log } Q_e - \frac{K1}{2.303}t \quad (3.8)$$

Where Q_e and Q_t (mg g^{-1}) are the amounts of As (III) adsorbed on the adsorbent at equilibrium and at different times t (min^{-1}). K_1 is the rate constant of the adsorption process (min^{-1}). Values of K_1 can be calculated from the slope of the plots of ln (Q_e – Q_t) versus *t*. and Qe was from the intercept.

3.13.2. Pseudo-Second-Order Kinetic Model

The pseudo-second-order kinetic model equation is usually described as follows

$$\frac{dQt}{dt} = K_2 (Qe - Qt)^2 \quad (3.9)$$

Which can be rearranged to obtain a linear form $\frac{t}{Qt} = \frac{1}{K2Qt^2} + \frac{t}{Qe}$ (4.0)

Where k_2 is the equilibrium rate constant of pseudo-second-order adsorption (g mg–1 min–1)

CHAPTER FOUR

4. RESULT AND DISCUSSION

4.1. Moisture Content Analysis

Table 3: Moisture contents of orange peels

	Sample orange peel(g)	Dry orange peel Weight(mg)	Moisture Content (%)	Average (%)
Moisture Content Determination	5	±1. 45	±0.29	
	5	±1. 41	±0.282	±29.86
	5	±1.47	±0.294	

Table 4: Ash content of orange peel

	Sample orange peel(g)	Residue(g)	Ash content (%)	Average (%)
Ash content	2	±1.45	±72.5	±71.76
	2	±1.42	±71.3	
	2	±1.43	±71.5	

From the result Table 3 and 4, orange peel sample had high percentage of moisture content it's about 29.86% and 71.76% noncombustible volatile matter. In general interpretation from the result, the composition of ash content in orange peel was high as compared to the total dry solid mass contained in the orange peels; deduce that orange peel varieties are not better in phytochemical. The presence of less amount of water vapor in the peel was important because it can reduce dissolved oxygen presence. As a result, it reduces the corrosion effect on the surface of nZVI.

4.2. Total Phenol Content of extract

Total polyphenol content (TPC) of orange peel extract was determined using the Folin–Ciocalteu method. Folin–Ciocalteu reagent, a mixture of phosphor-tungstic ($H_3PW_{12}O_{40}$) and phosphomolybdic ($H_3PMo_{12}O_{40}$) acids, is reduced to blue oxides of tungsten (W_8O_{23}) and molybdenum (Mo_8O_{23}) during phenol oxidation. This reaction occurs under alkaline

condition provided by sodium carbonate. The intensity of blue color reflects the quantity of polyphenol compounds, which can be measured using a 725nm using a UV-Visible Spectrophotometer (UV-7804C).

Table 5: Gallic acid standard solution and corresponding absorbance

Concentration of Gallic acid Standard(mg/L)	Average Absorbance
1	0.2227
2	0.5276
3	0.7675
4	1.0527
5	1.2657

Table 6: Sample solution Concentration and corresponding Absorbance

Sample solution Taken (µL)	Absorbance	Average Absorbance
50	1.0135 1.1145 1.1042	1.0774

The Gallic acid equivalent concentrations at 1.0774 absorbance were obtained using the Gallic acid standard calibration curve ($y = 0.2611x - 0.0161$, $R^2 = 0.9969$) as shown in the figure 4. Standard Gallic acid concentration equation Gallic acid equivalent concentrations (C) was obtained 4.188 mg/ml.

Total phenol contents (T) expressed in Gallic acid equivalent (mg of Gallic acid/g dry extract) was calculated by direct substitution in the relationship expressed in Eq 2.8. The total phenol contents were 31.41 mg of Gallic acid equivalent per gram of dry extract (157 mg GAE/g extract. Similar phenomenon was observed by other researchers according to the study (Hegazy and Ibrahium 2012), the result of total phenol content obtained was 169.56mg GAE/g extract for different varieties of orange peels.

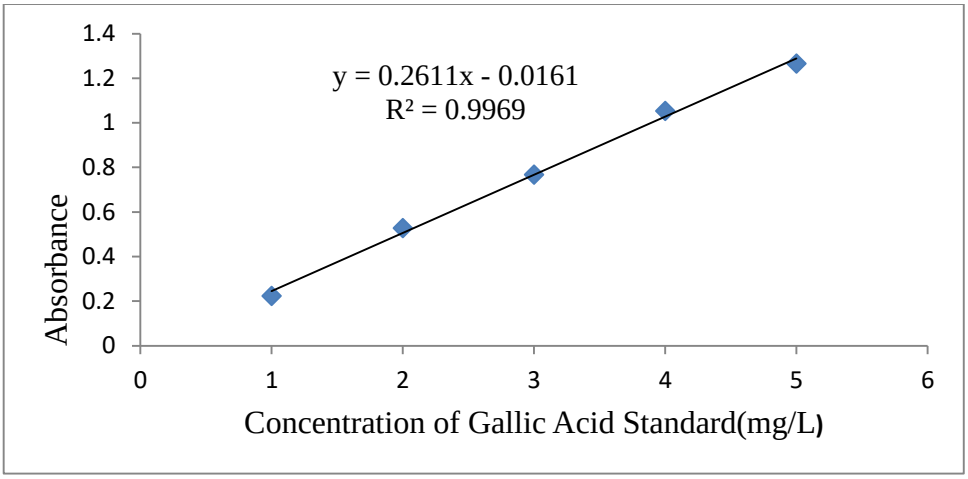

Figure 4: Gallic acid standard solution and corresponding Absorbance

4.3. FTIR Analysis on nZVI and Orange Peel Extract

FTIR analysis was performed to identify the existence of surface functional groups of orange peel extract and predict their role in the synthesis of nZVI. The functional groups of the Adsorbent were determined using Spectrum 65 FT-IR (PerkinElmer) in the wave range 4000-400cm-^{1}using KBr pellets. From figure (5,6), there is a prominent peak at 3464 corresponding to the polyphenols and it is seen that these phenolic groups are responsible for reducing Fe(III) to Fe(0). Another strong peak occurs in the range of 1700-1800 cm-1 corresponding to the carbonyl group which was responsible for reduction during the synthesis and also providing stability to the nanoparticle by acting as capping agents. The peak at 1641 cm-1 was due to attraction of some water molecules on the surface of the nZVI in the form of physical adsorption. The wave length at 639 cm^{-1} indicated to the presence of hematite (α-Fe2O3). The peaks at 3464 and 1641cm−1 were assigned to the O–H stretching vibration of polyphenols, partly were due to the O–H stretching vibration of FeOOH. the band at 698 cm-1 is due to the symmetric Fe-O stretch, and the broad band near 2078 cm-1 is attributable to the stretching mode of the bulk hydroxyl groups.

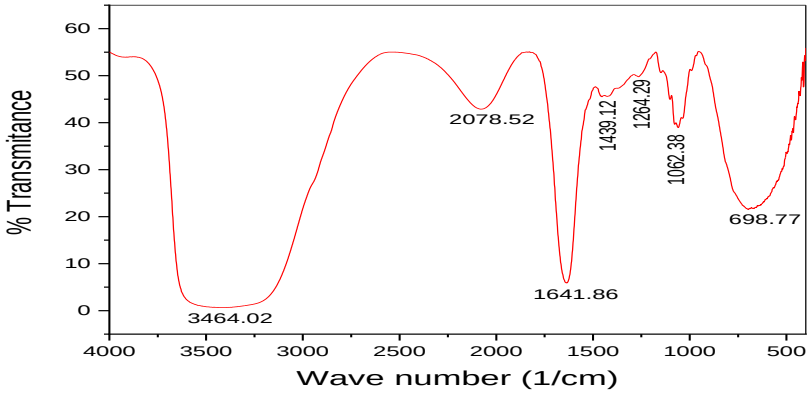

Figure 5: FT-IR plot of orange peel extract

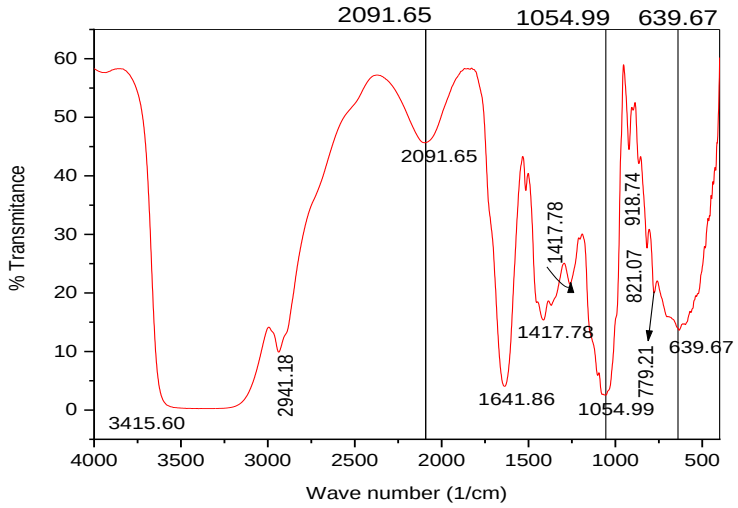

Figure 6: FT-IR plot of nZVI particle stabilized by CMC

4.4. XRD Analysis on CMC Stabilized nZVI

The XRD analysis of nZVI is shown in (Figure 7). This technique was used to determine the material and crystalline structure of iron nanoparticles. The spectra show that there was main peaks intensity of at 44.8° and 67.2°indicating the presence of nZVI dominant in the sample. The peak at 2Θ of 32.6° indicates the presence of Fe_2O_3 and low-intensity peaks in at 22° corresponding to the organic matter coated on the surface of nZVI (Fazlzadeh, 2017).

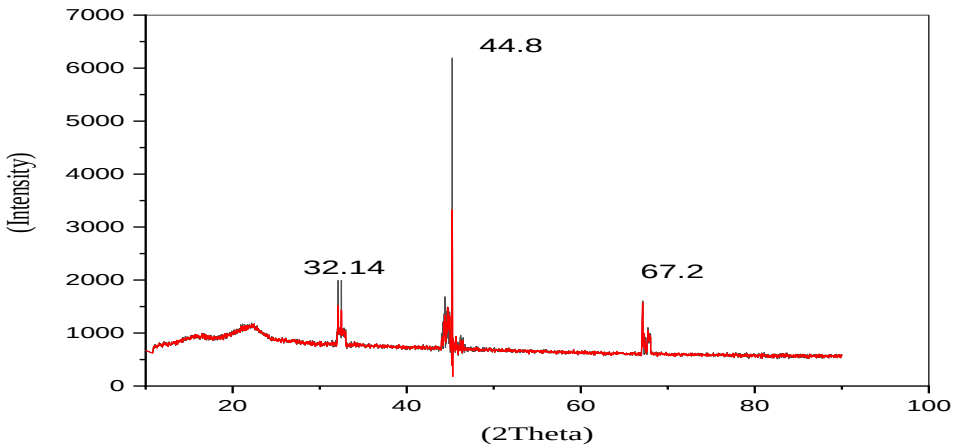

Figure 7 : XRD plot of greenly synthesized Iron nano particle stabilized by CMC

By applying Debye–Scherrer equation

$$D = k \lambda / \beta \cos\theta \qquad (4.1)$$

Where D is the mean size of crystallites (nm), K is crystallite shape factor (K = 0.9), λ is X-ray wavelength (λ = 0.15406 nm), β is full width at half the maximum (FWHM) in radians of the X-ray diffraction peak (β = 0.207) and θ is the Bragg angle (44.8°), the average nanoparticle size was found to be 41.5 nm. This result approximate with the data gained from

4.5. Scanning Electron Microscope

Fig 8 illustrated that the CMC-stabilized nZVI particles had a shape of euhedral, irregular, and square and the size of most of the individual particles was less than 100 nm. CMC kept nanoparticles physically separated and led to produce more stable nanoparticles. CMC could provide both electrostatic and steric repulsion to prevent particle aggregation. This observation could be caused by the rapid nucleation and crystal growth during the titration of a high amount of polyphenol in the reduction process. It showed also that coating the nanoparticles with the stabilizers greatly change the surface potential by enhancing the surface area. Fig 8 (b), the micrograph showed that the nanoparticles do not appear as discrete particles but form much larger dendritic flocs whose size could reaches micron scale. The non-stabilized nZVI particle appeared to be merge to one another possibly because of the strong magnetic dipole–dipole attractions between the non-stabilized individual nZVI particles (F. He, D. Zhao,2007).

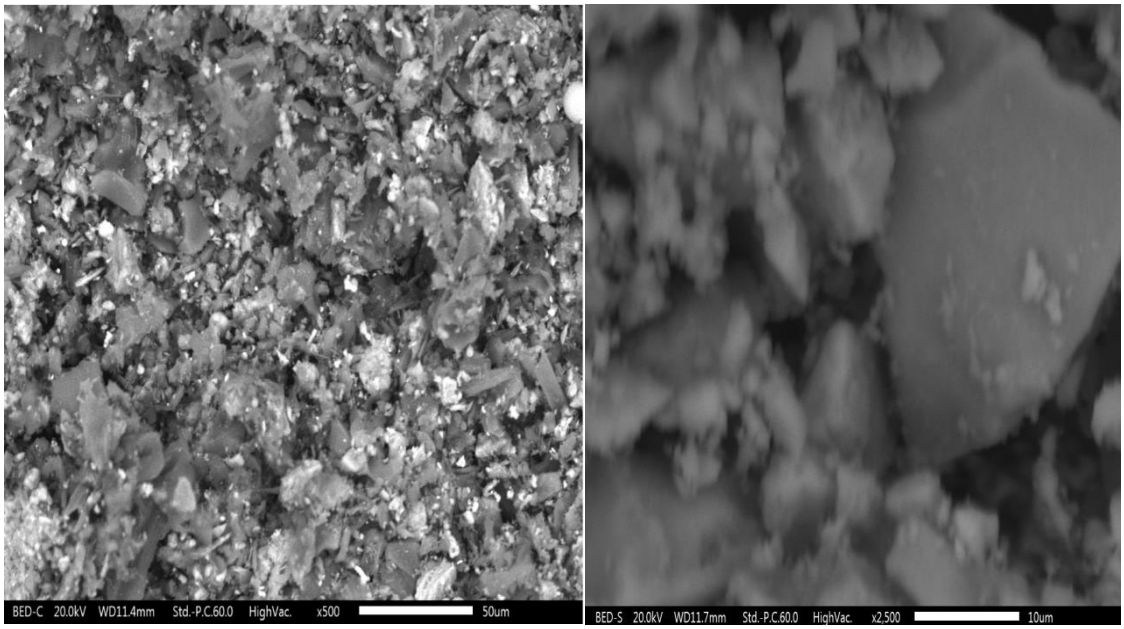

Figure 8 SEM image of nZVI (a) bare of non-stabilized nZVI (b) CMC-stabilized nZVI particles

4.6. Analysis of variance (ANOVA) for Design Model

General factorial design is usually focused on obtaining a model that definitively selects the vital process inputs, investigating interactions between the vital inputs, and making predictions about the process output. The standard analysis of a total number of 27experiments results using quadratic regression analyses. The effects of three independent variables that were adsorbent dosage, pH and initial concentration of As (III) with three levels were chosen as independent variables with designated factors as A, B, and C, respectively.

Table 7 Designed variables

Independent Variables	Range and Level Variables		
	Low	Medium	High
PH	2	6	9
Concentration(mg/L)	10	15	20
Dosage(mg)	0.5	1.0	1.5

4.7. Experimental Design Analysis

Table 8: Results and Discussion on Experimental Design Analysis

Source	Std. Dev.	Adjusted R-Squared	Predicted R-Squared	R-Squared	PRESS	
Linear	4.25	0.7368	0.7024	0.6333	579.56	
2FI	4.03	0.7944	0.7327	0.5452	718.86	
Quadratic	1.66	0.9703	0.9546	0.9134	136.89	Suggested
Cubic	1.44	0.9869	0.9658	0.8580	224.39	Aliased

Table (8), reveals about the fitting of the data to various models (linear, two factorials, quadratic and cubic) and analysis of variance showed that removal of As (III) using nZVI was properly described with a quadratic polynomial model. As shown in table (7) the Adjusted R^2 of the quadratic model (0.9703) is higher than that of linear (0.7368) and two factorial (0.7944) models. The cubic model was found to be aliased. Fitting of the data to various models (linear, two factorials, quadratic and cubic) and analysis of variance showed that the removal of As (II) by nZVI is well represented by second order quadratic regression mode.

Table 9: Analysis of Variance

Source	Sum of Squares	df	Mean Square	F Value	p-value Prob > F	
Model	1533.65	9	170.41	61.79	< 0.0001	Significant
A-As-Concentration	37.49	1	37.49	13.59	0.0018	
B-pH	984.05	1	984.05	356.83	< 0.0001	
C-Dosage	164.74	1	164.74	59.74	< 0.0001	
AB	16.07	1	16.07	5.83	0.0274	
AC	1.61	1	1.61	0.58	0.4559	
BC	73.43	1	73.43	26.63	< 0.0001	
A^2	57.47	1	57.47	20.84	0.0003	
B^2	77.29	1	77.29	28.03	< 0.0001	
C^2	143.28	1	143.28	51.95	< 0.0001	
Residual	46.88	17	2.76			
Cor Total	1580.53	26				

The Model F-value of 61.79 implies the model is significant. There is only a 0.01% chance that a "Model F-Value" this large could occur due to noise.Values of "Prob > F" less than 0.0500 indicate model terms are significant.In this case A, B, C, AB, BC, A^2, B^2, C^2 are significant model terms.Values greater than 0.1000 indicate the model terms are not significant. If there are many insignificant model terms (not counting those required to support hierarchy), model reduction may improve your model.

Table 10: Model Adequacy Checking

Std. Dev.	1.66	R-Squared	0.9703
Mean	86.16	Adj R-Squared	0.9546
CV%	1.93	Pred R-Squared	0.9134
PRESS	136.89	Adeq Precision	30.177

The R^2 = 0.9703 value provides a measure of how much variability in the observed response values can be explained by the experimental variable and their interaction. The R^2 value is always between 0 and 1. The closer the R^2 value is to 1, the stronger the model is and the better it predicts the response. In this case, the value of the determination coefficient (R=0.9703) indicates that 97% of the variability in the response could be explained by the model.

The "Pred R-Squared" of 0.9134 is in reasonable agreement with the "Adj R-Squared" of 0.9546.

"Adeq Precision" measures the signal to noise ratio. A ratio greater than 4 is desirable. Your ratio of 30.177 indicates an adequate signal. This model can be used to navigate the design space.

4.8. Development of Model equation

The empirical relationships between the response and the independent variables (A), concentration (B) pH (C) Dosage in terms of coded and actual factors can be determined by Design Expert software. The model equation that correlates the response (Y) to the extraction process variables in terms of coded factors after excluding the insignificant terms was given in equation.

Final Equation in Terms of Coded Factors:

Response Efficiency =+94.31
+1.45*A
-7.39 * B
+3.03* C
+1.15 * A * B
+0.37 * A * C
+2.47* B * C
-3.10 * A^2
-3.68 * B^2
-4.89* C^2

Final Equation in Terms of Actual Factors:

Response Efficiency = +54.43444
+3.49436 * As-Concentration
-1.20856 * pH
+35.21104 * Dosage
+0.065896* As-Concentration * pH
+0.14633* As-Concentration * Dosage
+1.40874* pH * Dosage
-0.12380 * As-Concentration^2
-0.30011 * pH^2
-19.54667 * Dosage^2

As shown in the final equation in terms of Actual factors, the response yield was affected by linear terms (A, B, C) and pure quadratic terms (A^2, B^2, and C^2) and interaction quadratic terms (AB, AC, BC). Linear terms of Concentration and Dosage were positive but the pH was negatively affected the response yield but the coefficients of interaction terms were positive but the response yield affected negatively by quadratic terms. From the linear effects, Dosage had highest effect on response yield. Similarly, pure quadratic term of dosage (C^2) had highest effect on response yield from negative quadratic effects.

Fig (9), A normal probability plot of the raw data is used to check the assumption of normality when using the t-test. In the analysis of variance, it is usually more effective (and straightforward) to do this with the residuals. If the underlying error distribution is normal, the plot will resemble a straight line

(Fig 10) showed that the relationship between actual and predicated values that actual values are the measured response data for a particular run, and the predicted values are evaluated from the model that are generated by using the approximately functions. The actual values distributed relatively near to the straight line, indicating good fitness of the model. Thus, the model developed is suitable for predicting the removal efficiency of Arsenic ion in the conditions investigated.

Again, in Figure (11), the plot of Interenally studentized residuals versus predicated was tested and the residuals were scattered randomly around ±3.00. This was an indication of better fitting of the model with the experimental data.

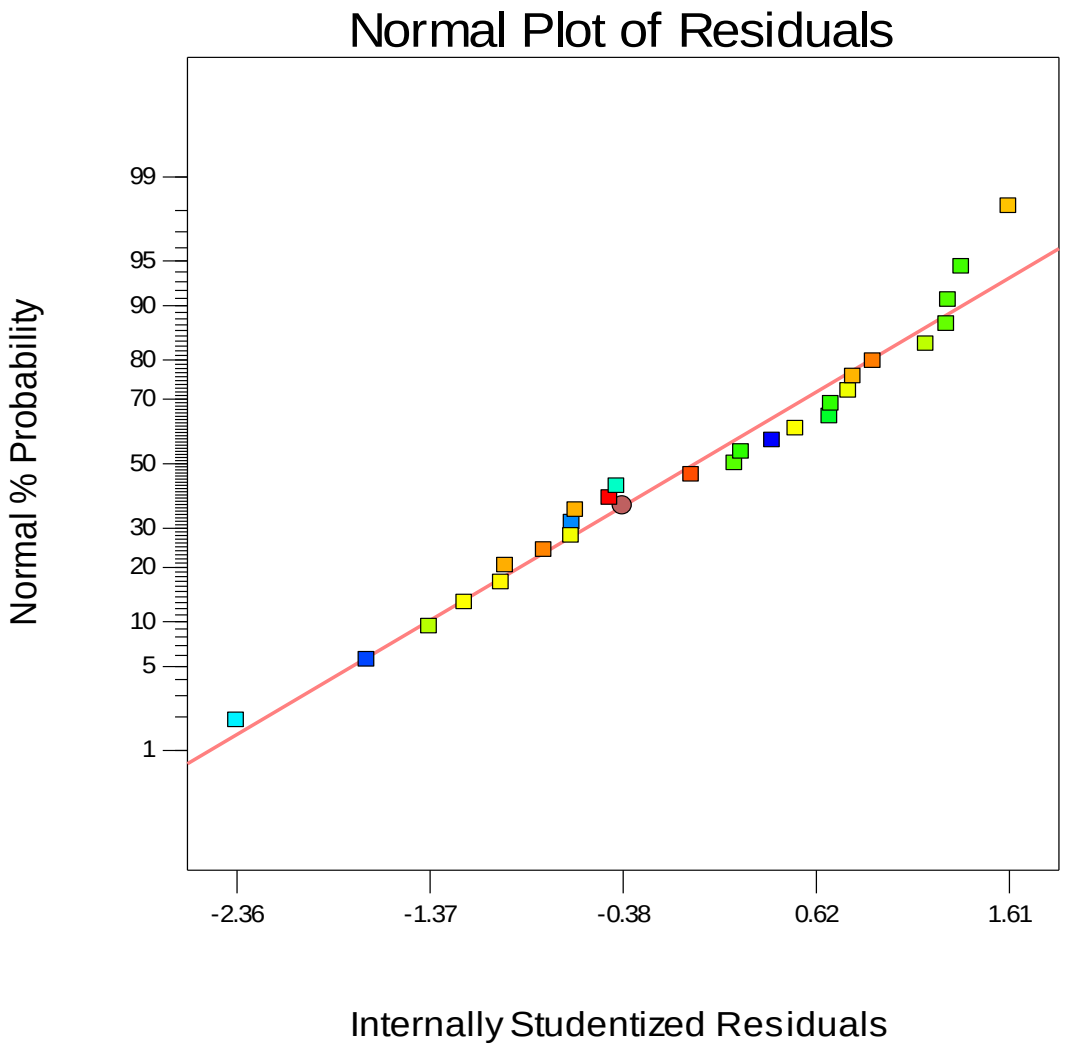

Figure 9: Normal Probability vs. Internally Studentized Residuals

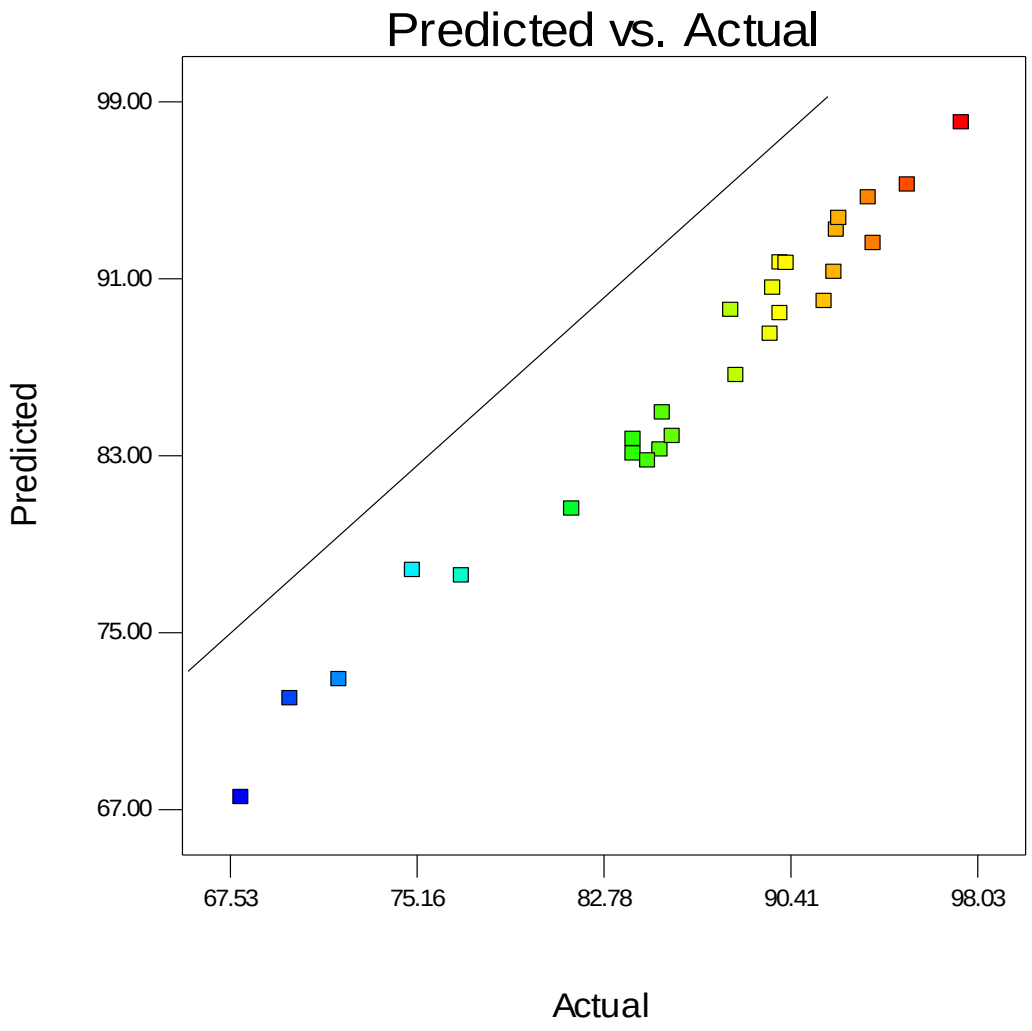

Figure 10: Predicated Vs. Actual

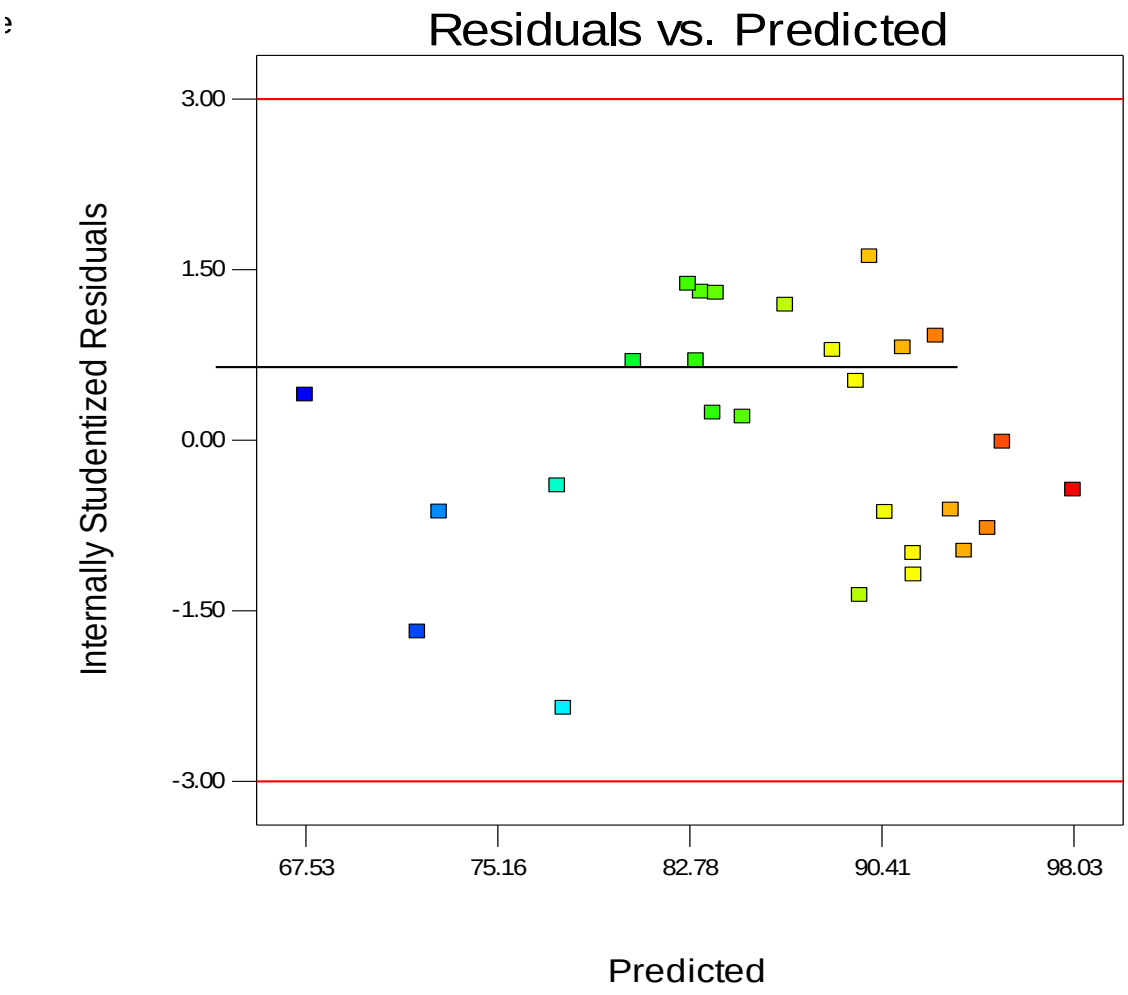

Figure 11: Internally Studentized Residuals vs. Predicated

4.9. Effect of Initial Concentration of As (III) on removal process

In this study, initial concentration of As (III) was varied from 10 to 20mg/l while maintaining other variable constant (adsorbent dose at 1.0 g and pH 6. The results of Figure (12) showed that the As (III) adsorption efficiency steadily increased linearly from 88.5% to 93.5% when the initial concentration increased from 10 to 15 mg/L and reaches a saturation stage beyond 15mg/L. At lower As (III) concentrations active sites of nZVI to solute concentrations ratio is higher as a result its concentration gradient greater. At higher As (III) concentrations the active sites of the adsorbent were occupied and becomes saturated. The effect of the initial As(III) concentration factor depends on the relation between the concentration of the As(III) and the available binding sites on an adsorbent surface(Rahmani, Ghaffari, and Samadi 2010)

.

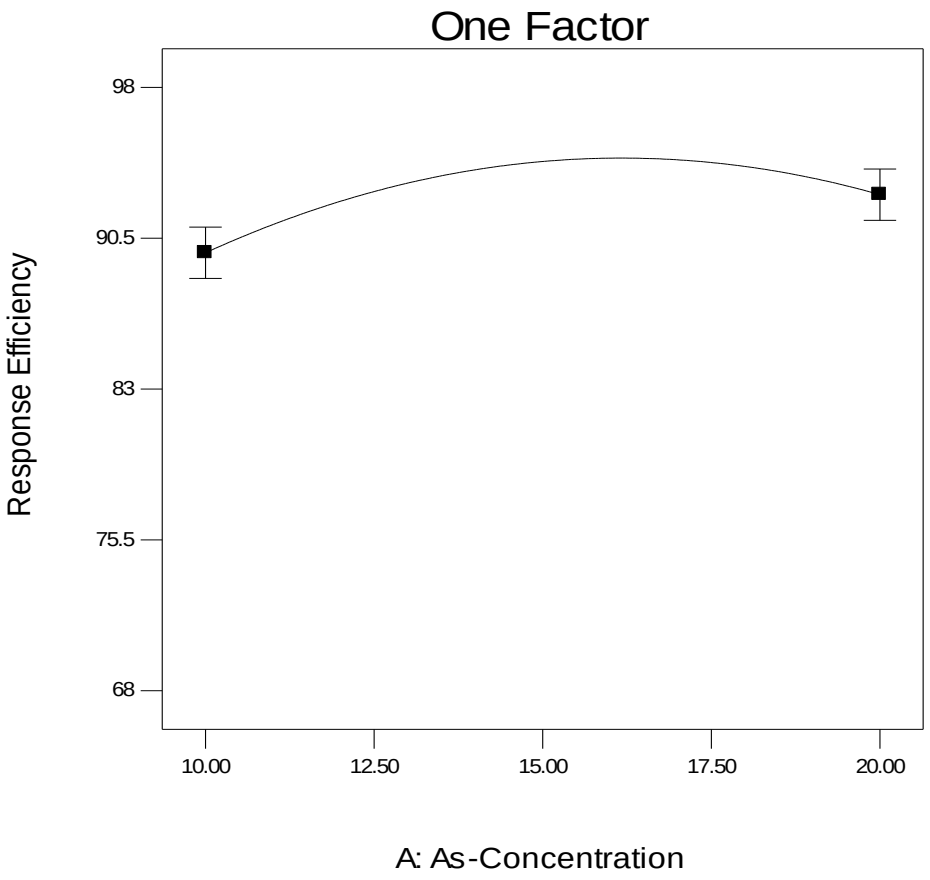

Figure 12 : Initial As (III) Concentration vs. Response Efficiency

4.10. Effect of pH

In this experiment, the adsorption behavior of As (III) ions was studied at different pH values, using 1g of nZVI particles with a fixed concentration As (III) (15 mg/L). The results obtained are shown in Fig (13) below, which shows that removal of As (III) ions increases with decreasing pH. It is due to when the ferrous ions dissolved from the iron surface collided with hydroxyl ions in alkaline solution, producing ferrous hydroxide precipitation on the iron surface occupying the reactive sites to hinder the reaction. Also accumulation of this precipitate on the outer side of the iron core decreases the surface area of the nZVI, which leads to decrease the mobility and reactivity, thereby limiting the radius of influence (Yaacob, Kamaruzaman, and Samsudin 2012).As (III) species can be predominant found as $H_2AsO_3^{-3}$ in alkaline solution while the nZVI corrosion product surfaces are also negative (Fe (III)-O) causing electrostatic repulsion. This means that acidic condition is the better for this process. pH also affected by dissolved oxygen presence this brought corrosion and which it

creates alkaline environment. The surface hydroxyl groups on the iron oxide can be protonated or deprotonated in solution depending on pH Capacity. Above pH 9.2, electrostatic repulsion may occur between dominant $HAsO_3^{2-}$ species and the deprotonated negatively charged nano-iron oxide surface, which hinders arsenic adsorption that decrease the efficiency of removal.

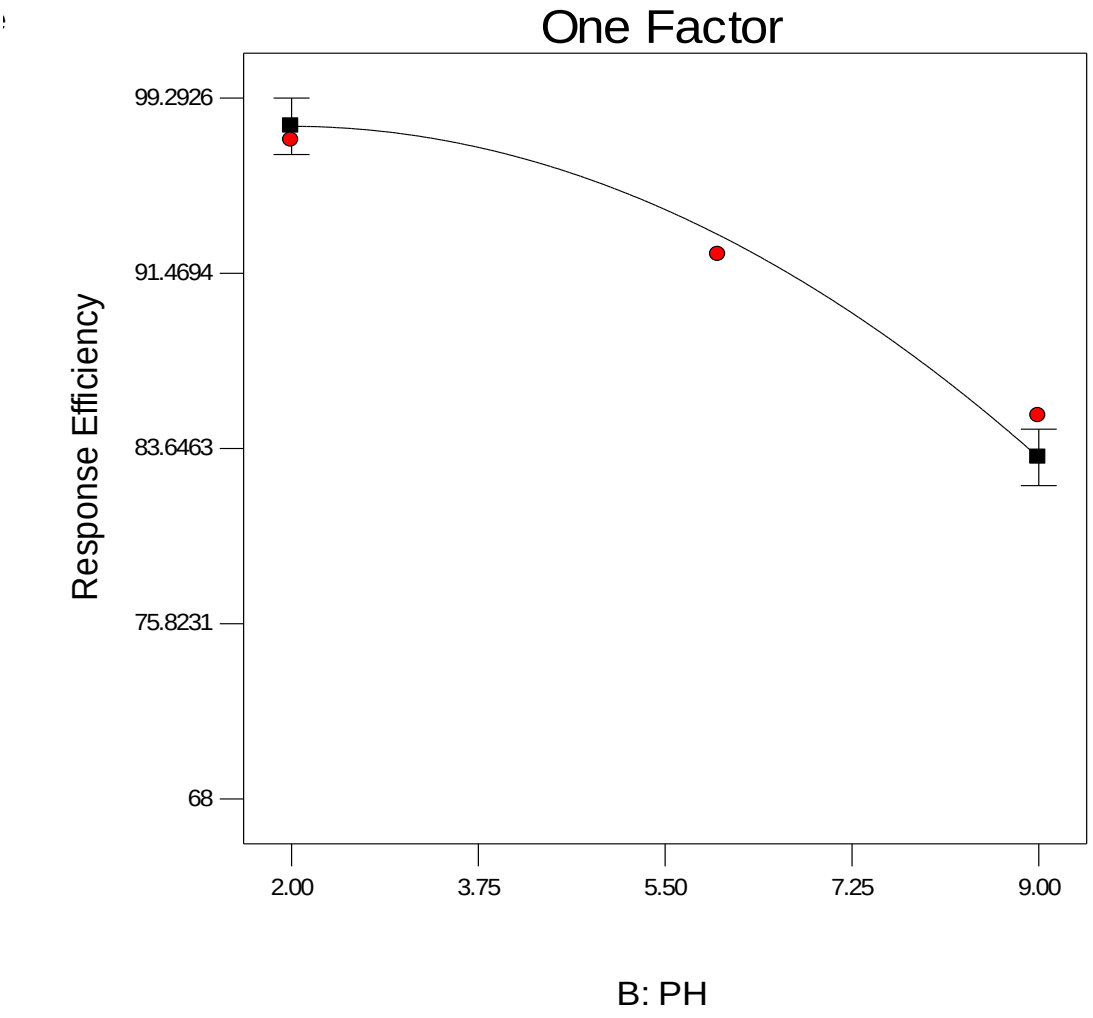

Figure 13: pH vs. Response efficiency

4.11. Effect of Dosage

Figure 14**,** shows the study on the effect of the amount of adsorbent on the process of adsorption were carried out by varying adsorbent dose from 0.5 to 1.5 g with pH 6 and with 15mg/L of initial concentration of As (III). The graph also indicated that the removal efficiency of As(III) ion increases from 84.8% to 93.7% when the amount of nZVI increased from 0.5 to 1g. With the increase of nZVI dose the absolute number of active sites increased,

resulting an increased overall adsorption efficiency of the systems. Any increment from 1g, the removal percentage of As (III) was slowly decreased this is due to particulate agglomeration. According to the Derjaguin-Landau-Verwey-Oberbeek (DLVO) theory, net interaction energy between particles resulted from the Van der Waals attraction force and the electrostatic repulsion force. When the attraction forces are higher than the repulsion forces, particles tend to aggregate. Moreover, these particles are also under magnetic attractive forces since they are made of zero-valent iron. Even CMC-stabilized nZVI particles had a tendency to agglomerate meaning the separate small particles cluster together to form larger particles or adhere due to magnetically attraction increase to each other. This decreases the surface area of the nZVI, which gradually decreases the mobility and reactivity, thereby limiting the radius of influence. which significantly reduce the removal efficiency. The aggregation is attributed to the magnetic forces among the iron particles. Similar phenomenon was observed by another researcher (Niu, 2005).

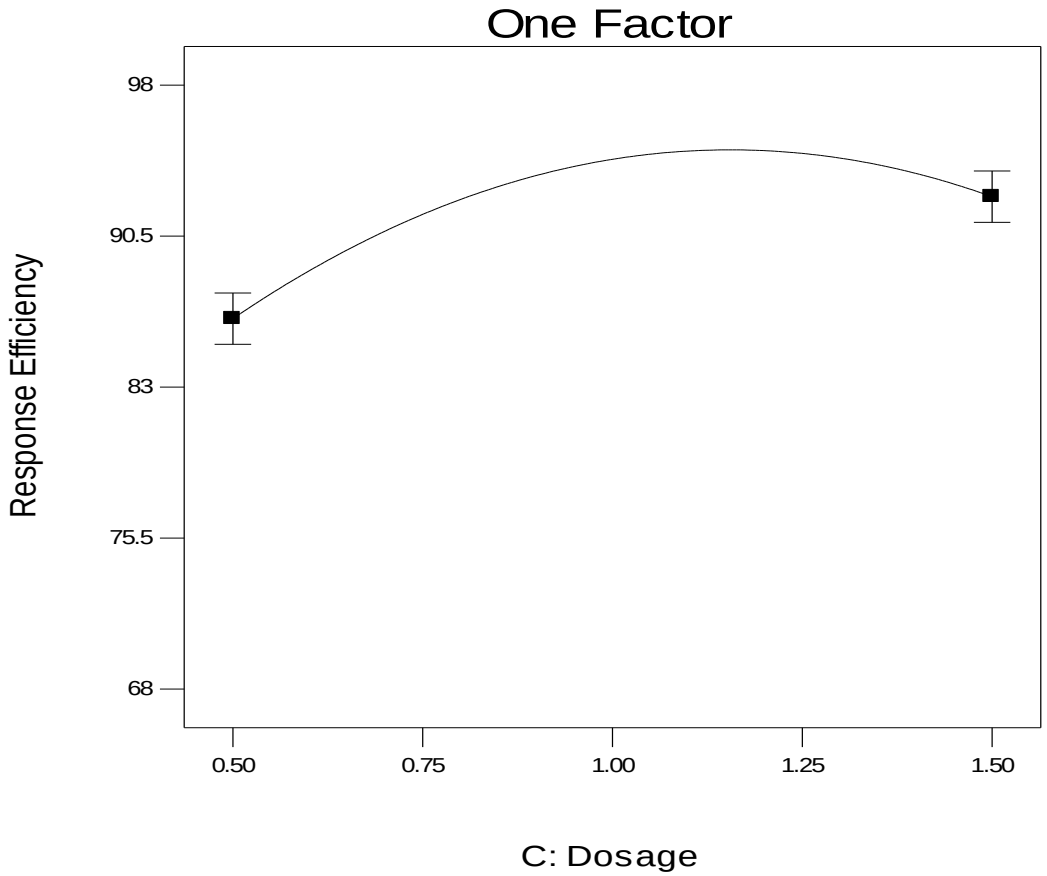

Figure 14: Effect of Dosage

4.12. Optimization of parameters for As (III) adsorption by Nano Zero Valent Iron

Table 11: Different alternative optimization solutions for As(III) removal from nZVI

Name	Goal	Lower Limit	Upper Limit	Lower Weight	Upper Weight	Importance
As-Concentration	is in range	10	20	1	1	3
PH	is in range	2	9	1	1	3
Dosage	is in range	0.5	1.5	1	1	3
Response Efficiency	Maximize	68	97.4	1	1	3

Table 12 : Optimizatized parameters for As (III) adsorption with its Desirebility

Solutions Number	As Concentration	pH	Dosage	Response Efficiency	Desirability	
1	14.11	2.81	1.06	97.6851	1.000	Selected
2	16.25	2.80	1.18	97.5831	1.000	
3	15.88	2.11	1.09	97.962	1.000	
4	15.44	3.34	1.19	97.4126	1.000	
5	13.90	2.74	1.00	97.5944	1.000	
6	17.30	2.19	0.97	97.4666	1.000	
7	16.62	3.06	1.14	97.5677	1.000	
8	16.67	2.71	1.13	97.6861	1.000	
9	15.18	3.51	1.09	97.4934	1.000	
10	13.46	2.64	0.99	97.4396	1.000	
11	17.01	3.17	1.12	97.4699	1.000	
12	15.22	2.71	1.12	97.8545	1.000	
13	15.18	2.65	1.08	97.9505	1.000	
14	15.81	2.91	0.98	97.7355	1.000	
15	13.33	2.63	1.01	97.4132	1.000	
16	16.22	2.30	0.97	97.8355	1.000	
17	14.77	2.87	1.09	97.8126	1.000	
18	13.67	2.12	0.94	97.5705	1.000	

19	14.91	2.53	1.01	97.9495	1.000
20	16.92	2.76	1.12	97.613	1.000
21	17.35	2.42	0.99	97.4792	1.000
22	15.91	2.73	1.00	97.8681	1.000
23	15.17	2.04	0.97	97.9775	1.000
24	17.02	2.93	1.00	97.5089	1.000
25	14.61	2.07	1.13	97.8158	1.000
26	13.48	2.28	1.01	97.6134	1.000
27	15.34	3.14	0.99	97.6201	1.000
28	17.01	2.42	1.10	97.6506	1.000
29	15.87	2.12	1.01	98.0005	1.000
30	13.76	2.21	1.16	97.4319	1.000

Based on the results the optimum possible solutions in adsorption of As (III) are presented in table 11, The goals of pH, initial concentration As (III),Dosage and Response efficiency all were set <in range> from lower and upper limits of their values. The upper and lower limits of the variables were specified and all variables were very significant and important due to their positive values from the developed regression model equation. The expert design under numerical optimization gave 30 different alternative optimizing solutions. The predicted optimum removal efficiency was 97.68% observed at possible parameters of 14.11mg/L,1.06 mg and 2.1 of concentration, dosage and pH respectively. Under these conditions the experimental removal efficiency was 97.4% which is close to the general factorial design optimal result of 97.68%, and this shows that the experimental values were found to be close to the predicted values and hence the model validation of the optimal solutions.

4.13. Analysis on adsorption Isotherm

For Langmuir Isotherm determination the value of Q_O and K_L were computed from the slope and intercept of the Langmuir plot of 1/Qe versus1/Ce. The data was tabulated using equation 3.3. Also, for Freundlich Isotherm determination, the value of K_f and 1/n were computed from the slope and intercept of the Frundlich Isotherm plot of Log Qe versus Log Ce. The data was tabulated using equation 3.6**.**

Table 13: Langmuir and Freundlich models for adsorption of As (III)

Langmuir Isotherm model			Freundlich Isotherm model	
Ce (g/L)	Qe(mg/g)	Ce/Qe(g/L)	LogCe(g/L)	LogQe
1.1	5.7	0.19	0.041	0.755
11	44	0.25	1.04	1.643
48	82.7	0.58	1.68	1.91
58	96.6	0.6	1.76	1.98
62	88.5	0.7	1.79	1.94

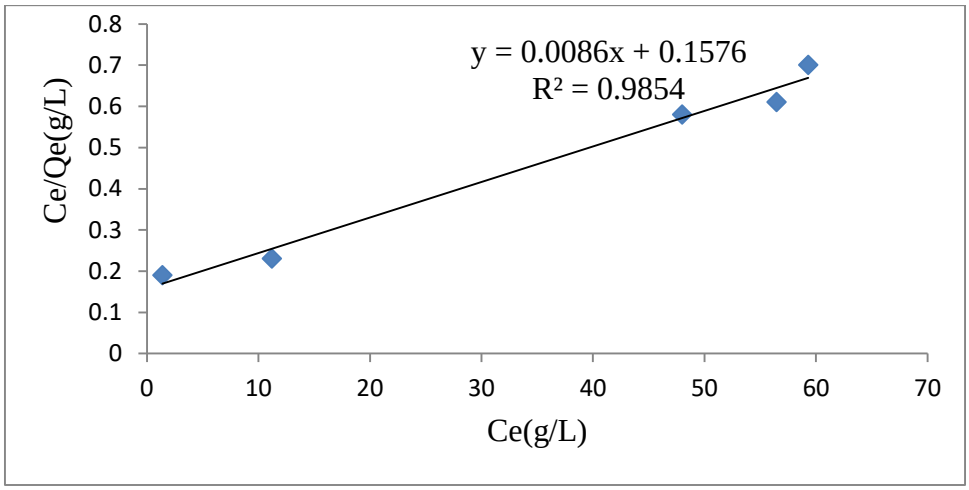

Figure 15: Langmuir Isotherm Adsorption for As(III)

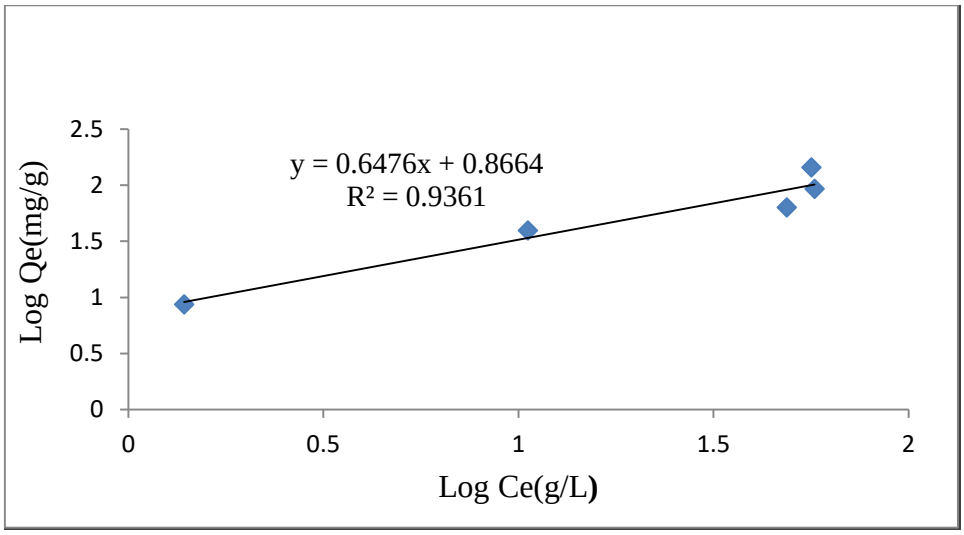

Figure 16: Fredundlich Isotherm Adsorption for As(III)

Table 14: Adsorption Isotherm Parameters

Langmuir Isotherm constant	Freundlich Isotherm Constant
Qo(max) =116.27mg/g	K_f =7.35mg/g
K_L =0.05 L/mg	1/n=0.647
R_L=0.64	R^2 =0.9361
R^2=0.9854	

Table 14: From the Freundlich's plots, the calculated values of K_f = 7.35mg/g and n =0.647. If an adsorbent has n value between 0 and 1 it is considered as a convenient adsorption and a good adsorbent. From the calculated results of the constants, it can be observed that the value of n is 0.647 which indicates that adsorption can be done in wide range of concentration, showing a satisfactory adsorption process. But the value of regression coefficient (R^2 = 0.9361) is lower than that of Langmuir isotherm value (R^2 = 0.9935). From table 14, the R^2 value for Langmuir isotherm model is closer to unity, which indicated that the Langmuir isotherm model was best fit in. The best fit of equilibrium data in the Langmuir isotherm expresses where once the heavy metal occupies the site no further adsorption takes place. According to Langmuir, the adsorption of solute from aqueous solution onto the adsorbents surface occurred as monolayer adsorption on the homogeneous number of exchanging sites. R_L value indicates the adsorption nature to be either unfavorable if R_L>1), linear if R_L =1, favorable if 0< R_L<1 and irreversible if R_L=0. From the data calculated in Table 14, the R_L is greater than 0 but less than 1 indicating that Langmuir isotherm is favorable. From this research work, the maximum monolayer coverage capacity (Q_o) from Langmuir Isotherm model was determined to be 116.2mg/g, K_L (Langmuir isotherm constant) is 0.05 L/mg, R_L (the separation factor) is 0.64 indicating that the equilibrium sorption was favorable and the R^2 value is 0.99 proving that the sorption data fitted well to Langmuir Isotherm model.

4.14. Kinetics of Arsenic (III) Adsorption

In all kinetic experiments, the pH of the solution and dosage was kept at optimum 2 and 15 respectively, and the sample was taken at every 20 minutes. The relationship between time and amount of As (III) adsorbed per nZVI adsorbent (mg/g) which is used to analyze

adsorption kinetics model. Figure 17, shows that Adsorption capacities of nZVI measured every 20 min time interval but two hours was needed to be reached at equilibrium (Qe =0.703mg/g).

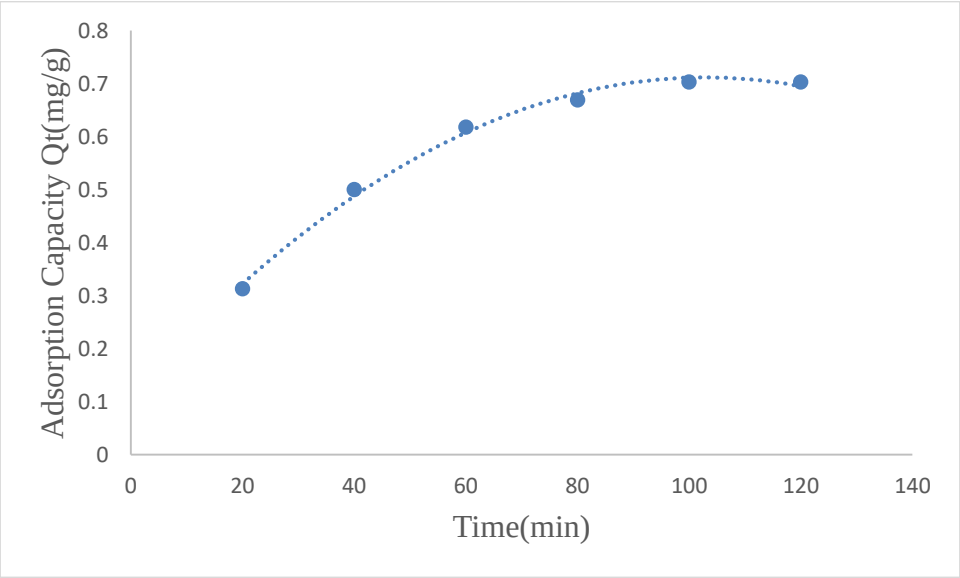

Figure 17: Adsorption capacities of nZVI measured at 20 min time interval

Kinetics of As (III) adsorption on nZVI were evaluated using pseudo-first- and -second-order models.

4.15. Pseudo First Order Sorption Kinetics

The plot of log (Qe - Qt) vs. t using equation 3.8 should give a linear relationship. The first-order rate constant K_1 (1/min) and the equilibrium capacity Log Qe can be obtained from the slope and intercept, respectively.

Table 15: Kinetic data for Pseud-First order Reaction rate

Time (min)	Final Concentration (mg/g)	Qt(mg/g)	Log (Qe-Qt) g min/mg	t/Qt g min/mg
20	10.3	0.313	-0.408	63.89
40	6.75	0.55	-0.815	77.72
60	5.75	0.618	-1.07	97.08
100	4.96	0.669	-1.468	119.58

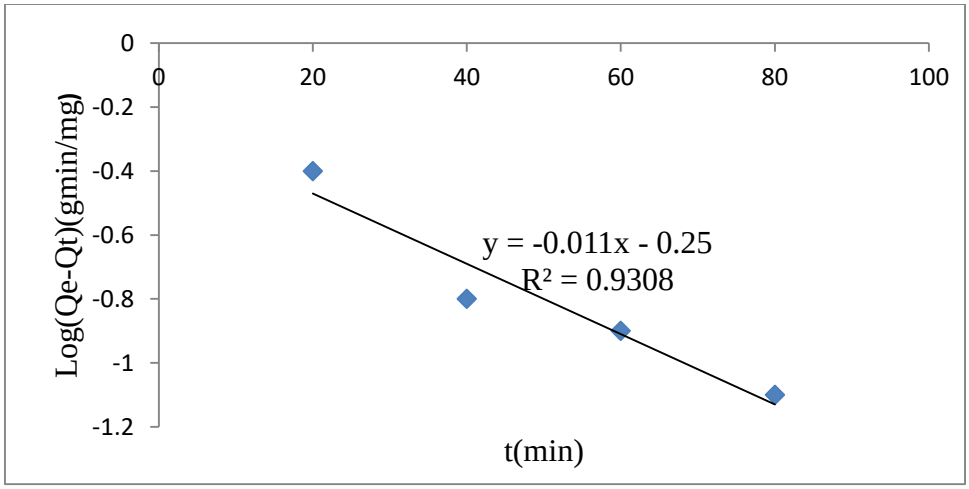

Figure 18: Pseudo first -order kinetic model adsorption (Adsorbent dosage=1g, initial Concentration = 15mg/L, pH=2)

4.16. Pseudo Second Order Sorption Kinetics

The plot of t/qt vs. t using equation 4.0 should give a linear relationship. The pseudo second order rate constant (K_2) and the equilibrium adsorption capacity (Qe) were calculate from the slope and intercept of the linear plot of t/Qt versus t for the nZVI adsorbent.

Table 16: Kinetic data for Pseudo-Second order Reaction rate

t(min)	Qt(mg/g)	t/Qt(min/mg/g)
20	0.313	63.9
40	0.55	72.7
60	0.618	97.1
80	0.669	119.6
100	0.703	142.2

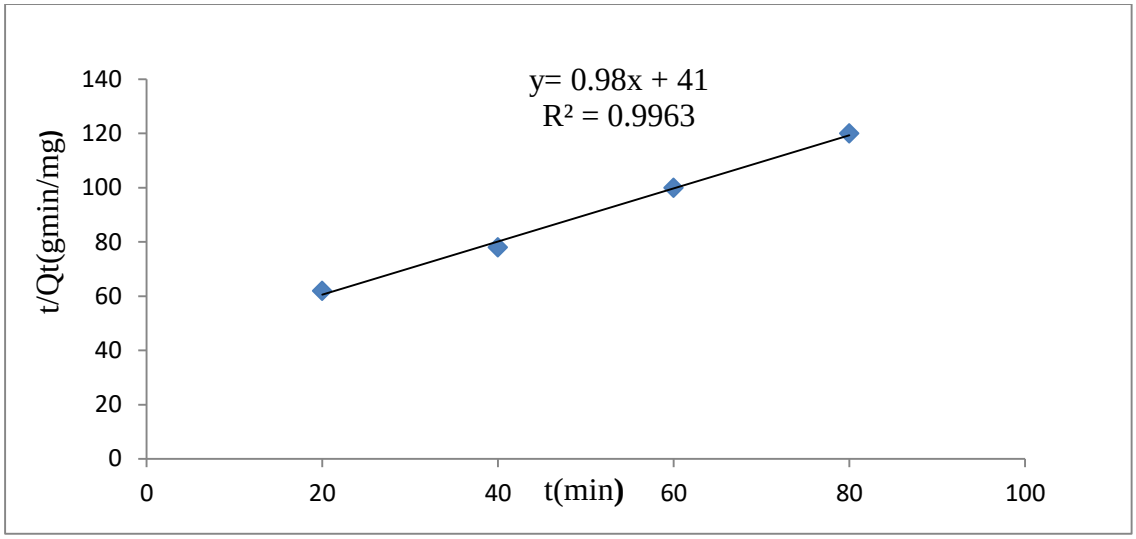

Figure 19: Pseudo Second Order Sorption Kinetics

Pseudo second-order kinetic model adsorption (adsorbent dosage=1g, initial concentration = 15mg/L, pH=2)

Table 17 : Adsorption kinetic model parameters of As (III) on the nZVI.

First order kinetic parameter	Second order kinetic parameter
Qe(mg/g)(cal) =1.02	Qe (mg/g)(cal) = 10.76
$K_1(min^{-1})$ =0.0274	$K_2(g.mg^{-1}.min^{-1})$ =0.0929
R^2=0.9308	R^2=0.9963

The two kinetic models were selected to study the adsorption kinetic of As (III) onto the surface of nZVI. From table 17, pseudo-second-order equation fitted the experimental data well with a correlation coefficient (R^2 =0.996) close to unity. The correlation coefficients suggested that the pseudo-second-order kinetic model fitted better for As (III) adsorption, which indicates that chemisorption took place during arsenic uptake. This implies that the adsorption rate was highly dependent on the availability of adsorption sites on nZVI surface rather than on arsenic (III) concentration in the solution. Moreover, it showed that the heterogeneity of the surface. Chemisorption occurs even at lower concentration; chemosorbed species are often irreversibly bound to the surface as a result they will not desorb under ambient temperature conditions(Cheng , 2016).

CONCLUSIONS

In this study, Nano scaled zero valent Iron was synthesized by polyphenol reduction method under atmospheric conditions. Synthesized nZVI characterization was carried out using XRD and FTIR techniques. The results showed that the spectra of XRD there was main peaks intensity of at 44.8° and 67.2ºindicating the presence of nZVI dominant in the adsorbent with the average nanoparticle size of 41.5 nm. SEM reveals that the size of most of the individual particles stabilized by CMC was less than 100 nm. CMC kept nanoparticles physically separated and led to produce more stable nanoparticles.

The experimental results have been fitted well by the Langmuir isotherm model with the higher correlation coefficients of R^2= 0.9854. Thus, indicating to the applicability of monolayer coverage of the As (III) on the surface of the nZVI.

The results indicated that removal percentage was found to be 91.6% for initial As (III) concentration of 15 mg/L, pH 2 and with dosage of 1.0g/L and about two hours is needed to reach the equilibrium for the adsorbent.

Kinetic results indicated that adsorption process followed the pseudo-second-order kinetic model with correlation coefficient (R^2 =0. 9963). This indicates that the adsorption rate was highly dependent on the availability of adsorption sites on nZVI surface rather than on arsenic (III) concentration in the solution. Generally, from the results obtained we can conclude that CMC-Stabilized nZVI is highly effective and environmentally friendly.

RECOMMENDATIONS

Based on this study I would like to forward that;

- ✓ In this study, nZVI was found to be a highly effective sorbent for the removal of arsenic (III).
- ✓ Bimetallic Nano scale particles are generally more reactive than the bare nZVI because the combination of metals increases the kinetics of the oxidation-reduction (redox) reaction.
- ✓ The effect of surface oxidation can be minimize using coating agent to ensure the presence corrosion of nZVI suspension.
- ✓ Impact of temperature on the synthesis and performance should be opened for further investigation
- ✓ Agitation speed has an impact during sensitizes of the nano particles such as in crystal growth and dispersion of particles.

REFERENCES

Azimi, Arezoo, Ahmad Azari, Mashallah Rezakazemi, and Meisam Ansarpour. 2017. "Removal of Heavy Metals from Industrial Wastewaters: A Review." *ChemBioEng Reviews* 4(1): 37–59.

Bezza, Fisseha Andualem, and Evans M. Nkhalambayausi Chirwa. 2018. "Production and Application of Zero Valent Iron Nanoparticles (NZVI) as Adsorbent for Removal of Chromium (VI) From Wastewater and Adsorption Studies." *Proceedings of the Water Environment Federation* : 4988–5003.

Chandra, Ch, and Fahmida Khan. 2017. "Green Synthesis of Nano Zerovalent Iron Using Glycine Max Leaf Extracts." *International Journal of Engineering Technology Science and Research* 4(8): 359–62. www.ijetsr.com.

Chen, Xunjun. 2015. "Modeling of Experimental Adsorption Isotherm Data." *Information (Switzerland)* 6(1): 14–22.

Cheng, Wei. 2016. "RSC Advances Etching Synthesis of Iron Oxide Nanoparticles for Adsorption of Arsenic from Water †.": 15900–910.

F. He, D. Zhao. 2007. "Manipulating the size and dispersibility of zerovalent iron nanoparticles by use of carboxymethyl cellulose stabilizers.". Envi- ron. Sci. Technol., 41, 6216–6221

Gautam, Deepti, and Bhuvanesh Gupta. 2009. "Arsenic Removal from Water : An Overview of Recent Technologies Author ' s Copy Arsenic Removal from Water : An Overview of Recent Technologies."

Hegazy, A E, and M I Ibrahium. 2012. "Antioxidant Activities of Orange Peel Extracts." 18(5): 684–88.

Hoag G. E., Collins J. B., Holcomb J. L., Hoag J. R., Nadagouda M. N., Varma R. S.2009. "Degradation of Bromothymol Blue by 'greener' Nano-scale Zero-valent Iron Synthesized Using Tea Polyphenols. Journal of Materials Chemistry"

Kozma, Gábor, Andrea Rónavári, Zoltán Kónya, and Ákos Kukovecz.2016. "Environmentally Benign Synthesis Methods of Zero-Valent Iron Nanoparticles." *ACS Sustainable Chemistry and Engineering* 4(1): 291–97.

Mu, Yi, Falong Jia, Zhihui Ai, and Lizhi Zhang. 2017. “Iron Oxide Shell Mediated Environmental Remediation Properties of Nano Zero-Valent Iron.” *Environmental Science: Nano* 4(1): 27–45. http://dx.doi.org/10.1039/C6EN00398B.

Nayana, C Hegde, and Tuppad Pushpa. 2016. “Nano Zero-Valent Iron for the Removal of Color and Chemical Oxygen Demand of Textile Effluent.” *Indian Journal of Advances in Chemical Science* S1: 236–38.

Nicomel, Nina Ricci.2015. “Technologies for Arsenic Removal from Water: Current Status and Future Perspectives.” *International Journal of Environmental Research and Public Health* 13(1): 1–24.

P, Kodal S. 2017. “Phenolic Pigment Extraction from Orange Peels: Kinetic Modeling.” (September).https://cest.gnest.org/sites/default/files/presentation_file_list/cest2017_00798_oral_paper.pdf.

Rahmani, A. R., H. R. Ghaffari, and M. T. Samadi. 2010. “Removal of Arsenic (III) from Contaminated Water by Synthetic Nano Size Zerovalent Iron.” *World Academy of Science, Engineering and Technology* 62(2): 737–40.

Suponik, Tomasz, Marcin Lemanowicz, and Pawel Wrona. 2016. “Stability of Green Tea Nanoscale Zero-Valent Iron.” 8.

Ulucan-Altuntas, K., E. Debik, and S. Gungor. 2018. “Nano Zero-Valent Iron Supported on Activated Carbon: Effect of Ac/Nzvi Ratio on Removal of Nickel Ion from Water.” *Global Nest Journal* 20(2): 424–31.

Vanderborght, B.M. & Van Grieken, R.E., 1977. “Enrichment of trace metals in water by adsorption on acitivated carbon. Analytical Chemistry.”49(2), pp.311–316

Vijayakumar, G, R Tamilarasan, and M Dharmendirakumar. 2012. “Adsorption , Kinetic , Equilibrium and Thermodynamic Studies on the Removal of Basic Dye Rhodamine-B from Aqueous Solution by the Use of Natural Adsorbent Perlite.” 3(1): 157–70.

Yaacob, Wan Zuhairi Wan, Noraznida Kamaruzaman, and Abdul Rahim Samsudin. 2012. “Development of Nano-Zero Valent Iron for the Remediation of Contaminated Water.” *Chemical Engineering Transactions* 28(January): 25–30.

Yang, Jinyue . 2019. “Nanomaterials for the Removal of Heavy Metals from Wastewater.”

Nanomaterials 9(3): 424.

Z. Wang, “Iron complex nanoparticles synthesized by eucalyp-tus leaves.2013.” ACS F. He, D. Zhao, “ Manipulating the size and dispersibility of zerovalent iron nanoparticles by use of carboxymethyl cellulose stabilizers, Envi- ron. Sci. Technol.”Sustainable Chemistry and Engineering,vol.1,no.12,pp.1551–1554,2013

APPENDICES

Table A-0-1: Concentration of Gallic acid Standard

Concentration of Gallic acid Standard(mg/L)	Absorbance	Average Absorbance
1	0.2424	0.2227
	0.2131	
	0.2126	
2	0.5115	0.5276
	0.5323	
	0.5391	
3	0.7544	0.7675
	0.7721	
	0.7761	
4	1.0478	1.0527
	1.0674	
	1.0429	
5	1.2031	1.2657
	1.2665	
	1.325	

Table A-0-2: Data used Calibration

Concentration	Absorbance
0	0
0.1	0.006
0.2	0.009
0.4	0.013
0.6	0.017
0.8	0.019
1	0.021
2	0.021
4	0.034
6	0.065

Table A-0-3: Removal Efficiency

Run	pH	Dosage (g)	Initial Concentration As(III) (mg/L)	Absorbance	Absorbance (Replicate)	Average absorbance (Response)	Removal Efficiency (%)
1	2	0.5	10	0.875	0.883	0.879	87.9
2	2	0.5	15	0.934	0.942	0.938	93.8
3	2	0.5	20	0.891	0.909	0.90	90.3
4	6	0.5	10	0.814	0.793	0.815	81.5
5	6	0.5	15	0.837	0.863	0.85	85.2
6	6	0.5	20	0.851	0.829	0.84	84
7	9	0.5	10	0.672	0.688	0.68	68
8	9	0.5	15	0.715	0.725	0.72	72
9	9	0.5	20	0.682	0.718	0.70	70
10	2	1.0	10`	0.933	0.939	0.936	93.6
11	2	1.0	15	0.978	0.97	0.974	97.4
12	2	1.0	20	0.955	0.949	0.952	95.2
13	6	1.0	10	0.867	0.913	0.891	89.6
14	6	1.0	15	0.918	0.922	0.922	92.3
15	6	1.0	20	0.972	1.008	0.991	90
16	9	1.0	10	0.768	0.774	0.771	77
17	9	1.0	15	0.842	0.864	0.853	85.1
18	9	1.0	20	0.853	0.839	0.846	84.6
19	2	1.5	10	0.932	0.904	0.918	91.8
20	2	1.5	15	0.953	0.929	0.941	91.4
21	2	1.5	20	0.912	0.932	0.922	92.2
22	6	1.5	10	0.871	0.893	0.882	88.2
23	6	1.5	15	0.923	0.882	0.9025	90.25
24	6	1.5	20	0.906	0.888	0.897	89.7
25	9	1.5	10	0.739	0.765	0.752	75
26	9	1.5	15	0.846	0.863	0.856	85.6
27	9	1.5	20	0.832	0.854	0.843	84

Table A-04 Prominent peaks and corresponding functional groups in FTIR spectra of orange peel-Fe Nanoparticle(Chandra and Khan 2017)

Peaks (cm-1)	Functional groups	Compound indicated
3491.44	O-H (H-bonded)	Polyphenols
1910.98	C=C asymmetric	Alkenes
1793.70	C=O stretch	Carbonyl Compounds
1704.35	C=O (H-bonded)	Carbonyl Compounds
1651.29	C=C(Symmetric)	Alkenes
1458.62	CH2 and CH3	deformation Alkanes
1380.44	O-H bending (in plane)	Polyphenols
1109.58	C-O stretch	Carbonyl Compounds
1042.57	C-O stretch	Carbonyl Compounds
983.93	C-O stretch	Carbonyl Compounds
947.63	=C-H and =CH2	bending Aromatics
877.82	=C-H and =CH2	bending Aromatics
833.14	=C-H and =CH2 bending	Aromatics

Figure A 0-1: Synthsizing Nano Zero Valent Iron using Polyphenol as a Reducing Agent

Figure A 0-2: (a), Scanning Electron Microscope (b) Probe horn sonicator at 50% amplitude power